



Pluvial periods in Southern Arabia over the last 1.1 million-years

Samuel L. Nicholson ^{a,*}, Alistair W.G. Pike ^b, Rob Hosfield ^a, Nick Roberts ^c, Diana Sahy ^c, Jon Woodhead ^d, Hai Cheng ^{e,f}, R. Lawrence Edwards ^e, Stéphane Affolter ^{g,h,k}, Markus Leuenberger ^g, Stephen J. Burns ⁱ, Albert Matter ^j, Dominik Fleitmann ^{a,k,**}

^a Department of Archaeology, University of Reading, United Kingdom

^b Department of Archaeology, University of Southampton, United Kingdom

^c Geochronology and Tracers Facility, British Geological Survey, Nottingham, United Kingdom

^d School of Earth Sciences, University of Melbourne, Victoria, Australia

^e Department of Earth Sciences, University of Minnesota, Minneapolis, MN, USA

^f Institute of Global Environmental Change, Xi'an Jiaotong University, Xi'an, China

^g Physics Institute, University of Bern, Switzerland

^h International Foundation for High Altitude Research Stations Jungfraujoch and Gornergrat, Bern, Switzerland

ⁱ Department of Geosciences, University of Massachusetts, USA

^j Institute of Geological Sciences, University of Bern, Switzerland

^k Quaternary Environmental Geology, Department of Environmental Sciences, University of Basel, Switzerland



ARTICLE INFO

Article history:

Received 31 May 2019

Received in revised form

22 November 2019

Accepted 26 November 2019

Available online 19 December 2019

Keywords:

Human dispersal

Middle east

Pleistocene

Speleothems

Arabia

Oxygen-isotopes

Carbon-isotopes

Water-isotopes

Uranium-series dating

Monsoon

ABSTRACT

Past climates and environments experienced by the Saharo-Arabian desert belt are of prime importance for palaeoclimatic and palaeoanthropological research. On orbital timescales transformations of the desert into a grassland landscape in response to higher precipitation provided “windows of opportunity” for hominin dispersal from Africa into Eurasia. On long timescales, palaeoenvironmental reconstructions for the region are predominantly derived from marine sediments and available terrestrial records from the Arabian Peninsula are limited to 450 ka before present (BP). Here, we present a new stalagmite-based palaeoclimate record from Mukalla Cave in Yemen which extends back to ~1.1 million years BP or Marine Isotope Stage (MIS) 31, as determined by Uranium-lead dating. Stalagmite Y99 grew only during peak interglacial periods and warm substages back to ~1.1 Ma. Stalagmite calcite oxygen isotope ($\delta^{18}\text{O}$) values show that every past interglacial humid period was wetter than the Holocene, a period in which large lakes formed in the now arid areas of southern Arabia. Carbon isotope ($\delta^{13}\text{C}$) values indicate habitable grassland environments developed during these pluvial periods. A total of 21 pluvial periods with precipitation of more than 300 mm yr^{-1} occurred since ~1.1 Ma and thus numerous opportunities for hominin dispersals occurred throughout the Pleistocene. New determinations of hydrogen (δD_{FI}) and oxygen ($\delta^{18}\text{O}_{\text{FI}}$) isotopes in stalagmite fluid inclusion water demonstrates that enhanced precipitation in Southern Arabia was brought by the African and Indian Summer Monsoons. When combined with sub-annual calcite analysis of $\delta^{18}\text{O}$ and $\delta^{13}\text{C}$, these data reveal a distinct wet (summer) and dry (winter) seasonality.

© 2019 Elsevier Ltd. All rights reserved.

1. Introduction

The Saharo-Arabian desert belt is a key-area for both palaeoclimatic and palaeoanthropological research. On orbital timescales, changes in the intensity and spatial extent of the African (ASM) and Indian Summer monsoons (ISM) transformed the Saharo-Arabian desert belt into a “green” landscape with abundant lakes (Drake et al., 2011; Fleitmann et al., 2011; Rosenberg et al., 2011, 2012; 2013; Bretzke et al., 2013; Larrasoña et al., 2013;

* Corresponding author. Department of Archaeology, Whiteknights Box 227, Reading, RG6 6AB, United Kingdom.

** Corresponding author. Department of Environmental Sciences, Bernoullistrasse 30/32, 4056 Basel, Switzerland.

E-mail addresses: s.l.nicholson@pgr.reading.ac.uk (S.L. Nicholson), dominik.fleitmann@unibas.ch (D. Fleitmann).

Matter et al., 2015; Breeze et al., 2016; Drake and Breeze, 2016). The timing and duration of these humid periods were pivotal “windows of opportunity” for hominin dispersals from Africa into Eurasia (“out-of-Africa”), which caused substantial demographic shifts during the last 130 ka (Timmermann and Friedrich, 2016; Bae et al., 2017). Knowledge of the “permeability” of the Saharo-Arabian desert belt on longer timescales could therefore be linked to potentially earlier hominin dispersals (e.g., Hershkovitz et al., 2018; Harvati et al., 2019). To date, two dispersals routes into Eurasia are favoured, the Levantine corridor (the *northern route*) and the narrow strait of Bab-al-Mandab (the *southern route*) (Fernandes et al., 2006; Fleitmann et al., 2011; Lambeck et al., 2011; Grant et al., 2012; Rohling et al., 2013; Breeze et al., 2016).

Marine sediments from the Mediterranean (ODP 967, Larrasoana et al., 2003; Grant et al., 2017), the Red Sea (KL 11, Fleitmann, 1997) Gulf of Aden (KL 15, Fleitmann, 1997; RC09-166, Tierney et al., 2017) and Arabian Sea (ODP 721/722, deMenocal, 1995; Clemens and Prell, 2003) provide long and continuous records of climate changes in the Saharo-Arabian desert belt, with a few extending back to the Pliocene. The majority of these records use terrigenous dust as a proxy for continental wetness, where reduced dust input and grain size data are related to enhanced vegetation cover during periods of higher precipitation (Fleitmann, 1997; Larrasoana et al., 2003). However, mobilisation, transport and deposition of dust is determined by multiple non-linear factors, such as production of dust, transport paths (wind direction), wind strength, erosion and vegetation density (Zabel et al., 2001). Terrestrial archives are thus required to test and mitigate uncertainties within marine dust records.

Terrestrial records from the main dispersal routes (Fig. 1) are primarily based on lacustrine sediments and speleothems (Burns et al., 2001; Armitage et al., 2007; Vaks et al., 2010; Fleitmann et al., 2011; Petraglia et al., 2011; Rosenberg et al., 2011, 2012; 2013; Jennings et al., 2015b), which cover only the last 350 to 450 ka before present (BP) (Rosenberg et al., 2013; Parton et al., 2018). While lake records provide information on the timing of these pluvial periods, it is much more difficult to use them for characterizing the climatic conditions at the time of their formation (Rosenberg et al., 2011, 2012, 2013). Palaeolake formations currently only provide limited “wet” or “dry” environmental information; comparison of climates among interglacial periods is much more challenging. Moreover, the nature of the lakes is the subject of debate, i.e. whether seasonal “wetlands” or perennial lakes existed (Enzel et al., 2015; Engel et al., 2017; Quade et al., 2018). Furthermore, palaeolake records from Arabia cannot currently be used to determine the source of moisture; a contentious issue within palaeoclimate research (Fleitmann et al., 2003b; Rosenberg et al., 2013; Kutzbach et al., 2014; Jennings et al., 2015b; Torfstein et al., 2015). Thus, an independent archive of continental wetness is required to elucidate these issues.

Speleothems (stalagmites, stalactites and flowstones) from the Arabian Peninsula and Middle East have great potential to deliver more comprehensive climatic records as they are protected from erosion. In addition, they can be used to extend the terrestrial palaeoclimate record beyond 600 ka using the Uranium–Lead (U-Pb hereafter) chronometer (Woodhead et al., 2006, 2012; Vaks et al., 2013, 2018). In arid regions such as Arabia, speleothem growth is dependent on both availability of moisture and vegetation respired CO₂ in soils (Burns et al., 1998; McDermott, 2004). The amount and source of precipitation are important controls on speleothem calcite δ¹⁸O_{ca} values (Dansgaard, 1964; Fleitmann et al., 2003a, 2011); whereas carbon isotopes (δ¹³C_{ca}) can provide information on the type (C₃/C₄ plants) and density of vegetation above the cave (McDermott, 2004; Cerling et al., 2011; Rowe et al., 2012). Finally, δD_{FI} and δ¹⁸O_{FI} values of water trapped in speleothem fluid

inclusion provide direct evidence of moisture sources when compared to modern isotopes in precipitation and regional meteoric waterlines (Bar-Matthews et al., 1996; Dennis et al., 2001; Meckler et al., 2015).

Previously published stalagmite records from Mukalla Cave in Yemen and Hoti Cave in Northern Oman (Fig. 1) extend back to ~330–300 ka BP, or Marine Isotope Stage (MIS) 9 (Fleitmann et al., 2011). The unique geographical position of Mukalla cave means speleothem growth occurs only when the northern limit of the monsoon rain belt passes ~14°N. Stalagmite Y99 (Mukalla Cave) is therefore an ideal specimen to track both meridional and zonal movements of the monsoon rain belt in southern Arabia and eastern Africa. Here, we present new Uranium–Thorium (²³⁰Th) and Uranium–Lead (U-Pb) dates for stalagmite Y99, which allows us to expand the Arabia terrestrial palaeoclimate record back to ~1.073 Ma, or MIS 31. Additional isotope measurements performed on Mukalla and Hoti Cave stalagmite calcite and fluid inclusion water allow us to track changes in the amount and source of rainfall.

2. Climatic and cave settings

Stalagmites presented in this study were collected from Mukalla Cave in Yemen and Hoti Cave in Northern Oman (Burns et al., 2001; Fleitmann et al., 2003b, 2011). Present-day climate in Southern Arabia is strongly governed by two major weather systems: The North Atlantic/Siberian pressure system in winter/spring and the African Summer Monsoon (ASM)/Indian Summer Monsoon (ISM) in summer (Fleitmann et al., 2003b). At present, hyper-arid to arid climate conditions prevail on the Arabian Peninsula and only the southernmost parts, such as the Yemen Highlands and Dhofar Mountains, are affected by the ASM and ISM.

2.1. Mukalla Cave, Yemen

Mukalla Cave (14°55'02"N; 48°35'23"E; ~1500 m above sea level, masl) is situated in the arid desert of Yemen, approximately 70 km north of Al Mukalla, Hadhramaut (Fig. 1). The current climate of Southern Yemen is dependent on the annual northward movement of the Intertropical Convergence Zone (ITCZ) and associated monsoonal rainfall belt. Annual precipitation is highly variable, yet averages ~120 mm yr⁻¹, mostly delivered in the spring and summer months (Mitchell and Jones, 2005). Bedrock thickness above the cave is approximately 30 m, and soil above the cave is mostly absent. No actively growing stalagmites were found when stalagmites Y99, Y97-4 and Y97-5 were collected in 1997 and 1999 respectively (Fleitmann et al., 2011), indicating that modern rainfall is too low to recharge the aquifer above Mukalla Cave. Based on these samples, Fleitmann et al. (2011) produced an environmental record up to MIS 9 (~330 ka), identifying four distinct growth intervals (GI I–IV) within stalagmite Y99. However, only the top section (collected in whole; Figs. 2B and S1) of a 3.2 m sample (Y99) was analysed. Here, remaining growth intervals from the lower part of Y99 (which was cored in several overlapping sections; Fig. 2C, S2 and S3), was dated to expand the terrestrial palaeoclimate record of Arabia. Calcite isotope measurements were performed throughout these growth intervals to characterise the climatic and environmental conditions during stalagmite growth. Additional calcite isotope measurements were performed at greater resolution in the top section of Y99.

2.2. Hoti Cave, Oman

Hoti Cave (23°05'N; 57°21'E; ~800 masl, Fig. 1) is located in the northern Oman mountains, where annual precipitation ranges

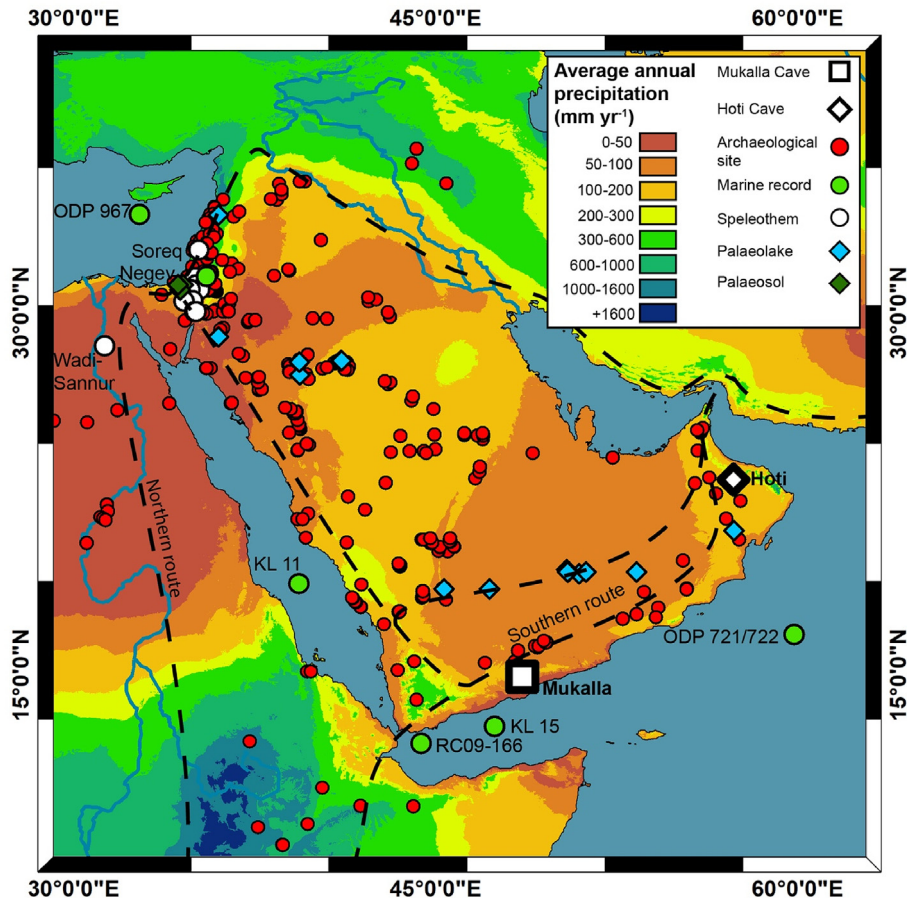


Fig. 1. Map of the Arabian Peninsula with present day (1970–2000) annual precipitation (accessible at: worldclim.org; Fick and Hijmans, 2017). Red circles denote Middle Palaeolithic archaeological sites (Bailey et al., 2015; Breeze et al., 2015; Groucutt et al., 2015a, 2015b; Jennings et al., 2015a; Petraglia et al., 2011; Rose et al., 2011). Dashed lines show potential hominin dispersal routes (Rosenberg et al., 2011). Also shown are caves (white circles; Bar-Matthews et al., 2003; El-Shenawy et al., 2018; Frumkin et al., 1999; Vaks et al., 2010); palaeolake sites (blue diamonds; Rosenberg et al., 2011, 2012, 2013; Petraglia et al., 2012; Matter et al., 2015), marine records (green circles; deMenocal, 1995; Fleitmann, 1997; Almogi-Labin et al., 2000; Larrasoana et al., 2003; Tierney et al., 2017), lake records (blue circles; Torfstein et al., 2015) and Mukalla and Hoti caves (white square and diamond, respectively; Burns et al., 1998, 2001; Fleitmann et al., 2003b, 2011). (For interpretation of the references to colour in this figure legend, the reader is referred to the Web version of this article.)

between 50 and 255 mm yr⁻¹ (station Al Hamra, 700 masl, 1974–1997). Precipitation is highly variable and mainly derived from three sources: the Mediterranean frontal system (December–March; Weyhenmeyer et al., 2002); orographic rain produced over the Jabal Akhdar Mountains during summer; and tropical cyclones, originating in the south-eastern Arabian Sea and the Bay of Bengal, every 5–10 years (Pedgley, 1969).

Stalagmites from Hoti Cave have been extensively studied (Burns et al., 2001; Neff et al., 2001; Fleitmann et al., 2003b, 2007). Several stalagmites cover the Holocene (samples H5, H12 and H14) and beyond (samples H1, H4, and H13). Stalagmite H13 is a ~3 m tall stalagmite covering MIS 5e, MIS 7e and MIS 9. Further details on the chronology and sampling location of Hoti Cave were presented in previous publications (Burns et al., 1998, 2001; Neff et al., 2001; Fleitmann et al., 2003b, 2007, 2011).

3. Methods

3.1. Dating

Stalagmites presented in this study were dated using the ²³⁰Th dating method back to ~550 ka and the U-Pb method for older samples (Woodhead et al., 2006; Cheng et al., 2013). The ²³⁰Th ages for Hoti Cave stalagmites are reported in Fleitmann et al. (2007, 2003a). For stalagmite Y99 (Mukalla Cave), a total of seventy ²³⁰Th

ages were determined back to approx. 550 ka BP (Tables S1–S3). Nineteen samples were analysed at the University of Minnesota (following the methods outlined by Cheng et al., 2013) and twelve additional samples were analysed at the British Geological Survey, Nottingham, UK (following the methods outlined by Crémière et al., 2016). Dates were calculated using the decay constant of Cheng et al. (2013), and a correction for the presence of initial ²³⁰Th was applied assuming a detrital U-Th isotope composition of ⁽²³²Th/²³⁸U) = 1.2 ± 0.6, ⁽²³⁰Th/²³⁸U) = 1 ± 0.5 and ⁽²³⁴U/²³⁸U) = 1 ± 0.5. The ages for GI XII and GI XVIII were determined via U-Pb methods. U-Pb ages for the lower part of Y99 were produced using both traditional solution-mode multi-collector inductively coupled plasma mass spectrometry (MC-ICP-MS) (following the methods detailed in: Woodhead et al., 2006) analysis (University of Melbourne, Australia) along with the recently developed Laser ablation (LA) method (BGS) (Tables S4 and S5). For LA-ICP-MS, the methods and analytical protocol follows that described by Coogan et al. (2016); U/Pb ratios were normalised to WC-1 carbonate (Roberts et al., 2017) and Duff Brown carbonate (Hill et al., 2016) was run as a check on accuracy.

3.2. Calcite oxygen and carbon isotope analysis

A total of 910 samples were collected along the main growth

axes of stalagmite Y99 GIs for stable isotope analysis. Samples were collected at resolutions of ~1 mm for growth phase I and II, ~2 mm for growth phases III–VII and ~5 mm for growth phases VII–XVIII (Table S6). Due to the variable size, visibility and direction of independent growth layers, it was not possible to produce Hendy tests. To provide further support for our Growth Interval assignments, additional samples were collected across visible growth discontinuities at 1 mm resolution within the lower sections of Y99 (Table S7; Fig. 2). Furthermore, H13 (Hoti Cave) was selected for sub-annual isotopic analysis to examine seasonality, due to its annual laminations. Samples were collected at 0.1 mm resolution (Table S8).

Isotope measurements were performed using a Finnigan Delta V Advantage Isotope Mass Spectrometer (IRMS) coupled to an automated carbonate preparation system (Gasbench II). Precision (1σ) is $\leq 0.2\text{\textperthousand}$ for $\delta^{18}\text{O}$ and $\leq 0.1\text{\textperthousand}$ for $\delta^{13}\text{C}$. Measurements were performed at the Chemical Analysis Facility (CAF), University of Reading, UK, and the Institute of Geological Sciences, University of Bern, Switzerland. Isotope values are reported relative to the Vienna PeeDee Belemnite (VPDB) standard.

3.3. Fluid inclusion deuterium and oxygen isotope analysis

Deuterium (δD_{FI}) and oxygen ($\delta^{18}\text{O}_{\text{FI}}$) isotopes of speleothem fluid inclusion water were analysed at the Physics Institute, University of Bern, Switzerland, using a recently developed extraction method (Affolter et al., 2014, 2015). Sixteen calcite blocks of $\sim 25 \times 5 \times 5$ mm (L, W, H) for fluid inclusion analysis were collected from Y99, H13 and H5. Samples were placed into a copper tube and connected to the measuring line, heated to ~ 140 °C and crushed, the liberated water was then transported to a wavelength scanned cavity ring down spectroscopy system (Picarro L2401-i analyser) under humid conditions (with standardised water of known isotopic composition) to prevent fractionation and minimize memory effects. The crushing of samples released, on average, $\sim 1 \mu\text{l}$ of water. Precision is 1‰ for δD_{FI} and 0.2‰ for $\delta^{18}\text{O}_{\text{FI}}$. Fluid inclusion values are reported on the Vienna Standard Mean Ocean Water (V-SMOW) scale (Table S9).

4. Results and discussion

This section is divided into two parts. In the first part we focus

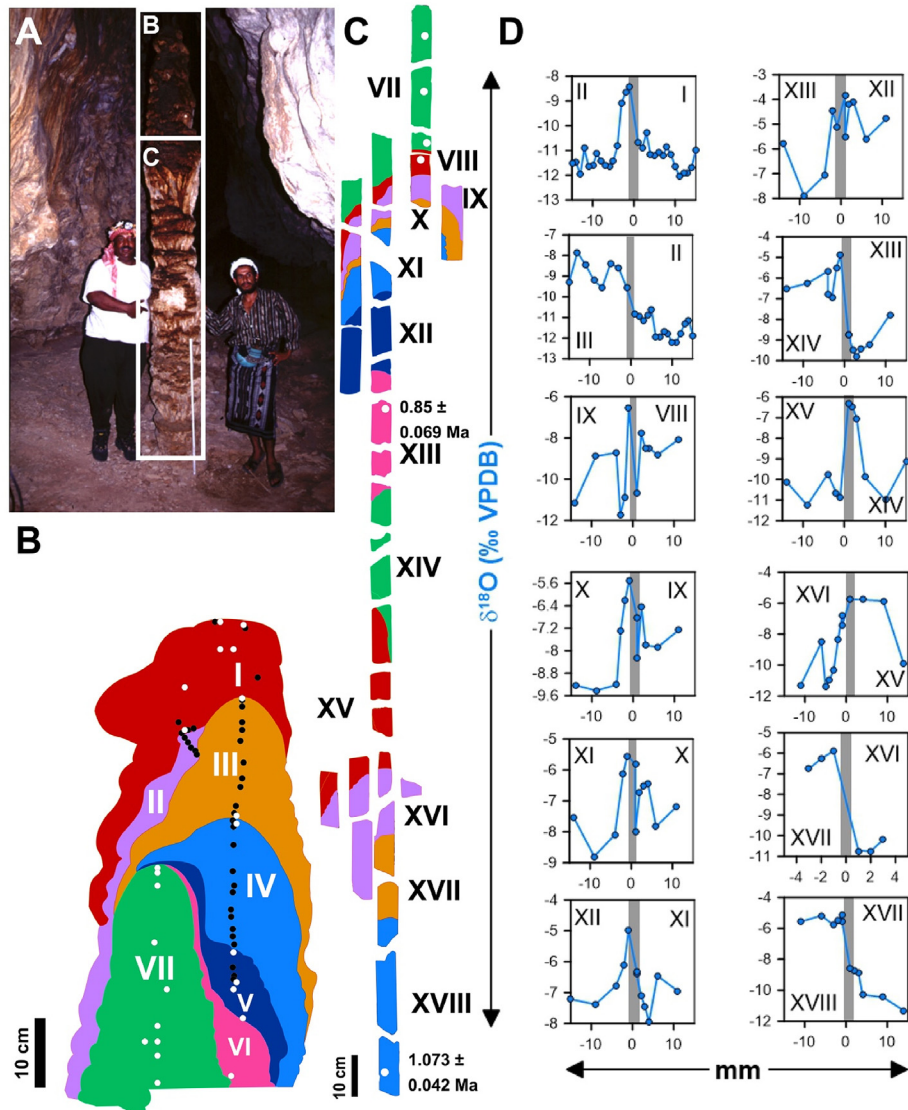


Fig. 2. (A) Stalagmite Y99 *in situ* in Mukalla Cave. (B and C) Y99 consecutive growth intervals (Figs. S1–S3). Location of ^{230}Th and U-Pb ages marked by black (Fleitmann et al., 2011) and white (this study) circles. (D) Plots show $\delta^{18}\text{O}_{\text{ca}}$ shifts over discontinuities between GIs (Tables S6 and S7).

on rainfall variability during the last 350 ka. We provide additional and more precise ^{230}Th ages for Y99 (Mukalla Cave), as well as stable isotope analysis of calcite and fluid inclusion water from Y99 (Mukalla Cave), H5 and H13 (Hoti Cave). We combine these ages with previously published Mukalla and Hoti Cave speleothem data to discuss the timing and environmental conditions of South Arabian Humid Periods (SAHPs) since 350 ka BP. By comparing our multiproxy records with marine and terrestrial palaeoclimate records from the African and Asian monsoon domains, we show that periods of enhanced rainfall and speleothem growth in Southern Arabia are related to a strengthening and greater spatial extent of the ASM and ISM during peak interglacials and interstadials. Within the second section, we provide an extended chronology and $\delta^{18}\text{O}_{\text{ca}}$ and $\delta^{13}\text{C}_{\text{ca}}$ stable isotope data for the lower portion of Y99 (Fig. 2C) in order to characterise humid periods in Southern Arabia back to ~ 1.1 Ma BP, making the stalagmite Y99 record one of the longest continental records from Southern Arabia.

4.1. Timing and nature of SAHPs during the last 350 ka

4.1.1. Chronology of Y99 GI I to V

The chronology of Y99 growth phase I to V is based on a total of 53 ^{230}Th ages (Fig. 3). These include 38 ages presented in Fleitmann et al. (2011) and 15 additional more precise ^{230}Th ages analysed for this study (Tables S1 and S2). Stalagmite Y99 GIs I-V coincide with peak interglacial periods and interstadials corresponding to MIS 5e, 7a, 7e, 9c and 9e (Fig. 4) when Southern Arabia was affected by the ASM and ISM (Fleitmann et al., 2011; Rosenberg et al., 2013). While age reversals are observed in GI IV and V, kernel probability density plots of all ^{230}Th ages obtained from Mukalla Cave (Y99, Y97-4, -5) and Hoti Cave (H1, H4, H5, H10, H11 and H14) indicates Y99 growth was more likely to occur within MIS 9c and 9e (Fig. 3).

4.1.2. SAHPs in Oman and Yemen during the last 350 ka

Growth intervals of stalagmites from Mukalla and Hoti Caves mark climatic intervals when effective precipitation was high enough to recharge the aquifers above both caves (Burns et al.,

2001; Fleitmann et al., 2003b, 2011; Fleitmann and Matter, 2009). At present, total annual rainfall averages $\sim 120 \text{ mm yr}^{-1}$ and $\sim 180 \text{ mm yr}^{-1}$ at Mukalla and Hoti Cave respectively, and actively growing stalagmites are either absent (Mukalla Cave) or very rare (Hoti Cave) (Burns et al., 2001; Fleitmann et al., 2003a, 2007, 2011). Thus, the existence of very tall and large diameter stalagmites such as H13 and Y99 (Fig. 2) in both caves is clear evidence that precipitation was considerably higher than today when they were formed (Vaks et al., 2010; Fleitmann et al., 2011; El-Shenawy et al., 2018). Based on the spatial distribution of actively growing stalagmites in the Levant and Negev – areas with very similar climatic conditions compared to Yemen and Oman – precipitation should have been around 300 mm yr^{-1} or greater to recharge the groundwater and trigger growth of stalagmites (Vaks et al., 2010, 2013). Considering the height and diameter of stalagmites Y99 and H13 (Fig. 2), precipitation was most likely considerably higher than 300 mm yr^{-1} . Intervals of speleothem growth at both cave sites are therefore a first indicator for continental wetness in Southern Arabia. An important feature of stalagmites Y99 and H13 is that their growth was reactivated multiple times, suggesting that the long-lasting cessations of stalagmite growth are related to arid climatic conditions (Burns et al., 2001; Fleitmann et al., 2011).

Over the last 350 ka BP, stalagmite growth in Mukalla and Hoti Caves (Fig. 4) occurred during peak interglacial periods and warmer substages corresponding to the early and mid-Holocene, MISs 5a, 5c, 5e, 7a, 7e, 9c and 9e (Fig. 4; Burns et al., 2001; Fleitmann et al., 2003a, 2003b, 2011; Fleitmann and Matter, 2009). SAHPs were related to intensified African and Indian summer monsoon circulation and a northward displacement of the tropical rain-belt and ITCZ at times of high boreal summer insolation and low ice volume (LR04 stack) (Burns et al., 1998, 2001; Fleitmann et al., 2011; Beck et al., 2018). Both the timing and frequency of SAHPs over the last 350 ka are in excellent agreement with other marine and terrestrial hydroclimate records from the Saharo-Arabian desert belt (Fig. 4). In the Gulf of Aden, low $\delta D_{\text{leafwax}}$ values in Core RC09-166 (Fig. 4) indicate greater rainfall in the Horn of Africa and Afar regions during the early to mid-Holocene (SAHP 1), MIS 5a, 5c, 5e (SAHPs 2–4) and MIS 7a (SAHP 5) (Tierney et al., 2017). Two aeolian dust records from the Gulf of Aden (KL 15) and central Red Sea (KL 11) show generally lower median grain size values during peak interglacial periods when erosion and mobilisation of dust was significantly reduced as a result of a denser vegetation cover in North Africa and Arabia (Fleitmann, 1997). Similarly, speleothem growth in Southern Arabia and Northern Egypt (Wadi Sannur Cave) are in good agreement, occurring at MIS 5e, MIS 7c and MIS 9c and 9e (El-Shenawy et al., 2018). Absence of speleothem growth in Northern Egypt during relatively warm substages (MIS 5c and 5a and MIS 3) suggests that ASM rainfall did not reach far into Egypt, highlighting a degree of regional and temporal variability. Sapropel layers in the Eastern Mediterranean are an additional proxy for ASM and ISM intensity and were mainly deposited during periods of increased Mediterranean rainfall and significantly higher monsoon precipitation in the Ethiopian highlands and resultant higher Nile discharge (Fig. 4; summarized in Rohling et al., 2015; Grant et al., 2016). The timing of SAHPs 1 to 8 is in excellent agreement with sapropels records, with the exception of the “ghost sapropels” 2 and 6 which are most likely not associated with higher Nile discharge (Rohling et al., 2015). Further north, the Soreq and Peqiin Cave $\delta^{18}\text{O}_{\text{ca}}$ records from the Levant are also sensitive recorders of changes in $\delta^{18}\text{O}$ of eastern Mediterranean surface seawater related to Nile discharge (Bar-Matthews et al., 2003; Rohling et al., 2015), with more negative $\delta^{18}\text{O}_{\text{ca}}$ values indicating higher Nile discharge during peak interglacial and interstadial periods (Fig. 4). Likewise, speleothem-based Negev Humid Periods (NHPs; based on speleothem ages) 1–4 are synchronous to SAHPs (Fig. 4), with the

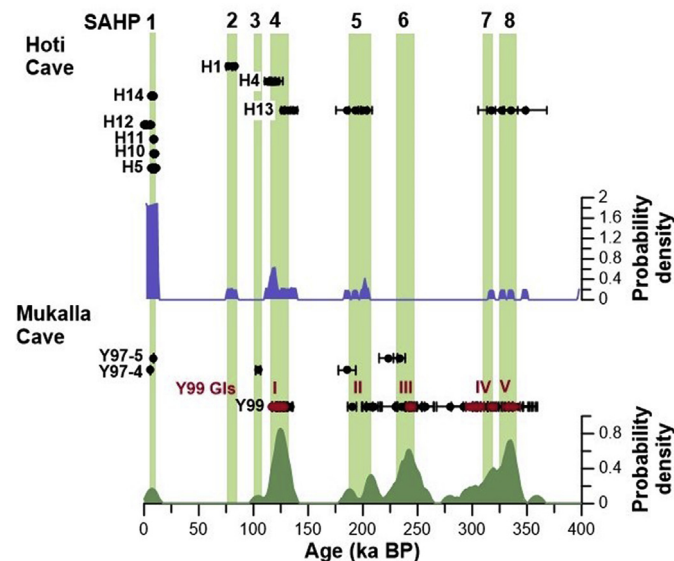


Fig. 3. ^{230}Th ages of Hoti Cave and Mukalla Cave speleothems. Red dots denote new Y99 ^{230}Th ages determined for this study. Age kernel probability density plots of Hoti (blue; 5 pt moving average) and Mukalla (green) and green bars show periods of most likely speleothem deposition. These were used to assign South Arabian Humid Periods (SAHP) 1–8. (For interpretation of the references to colour in this figure legend, the reader is referred to the Web version of this article.)

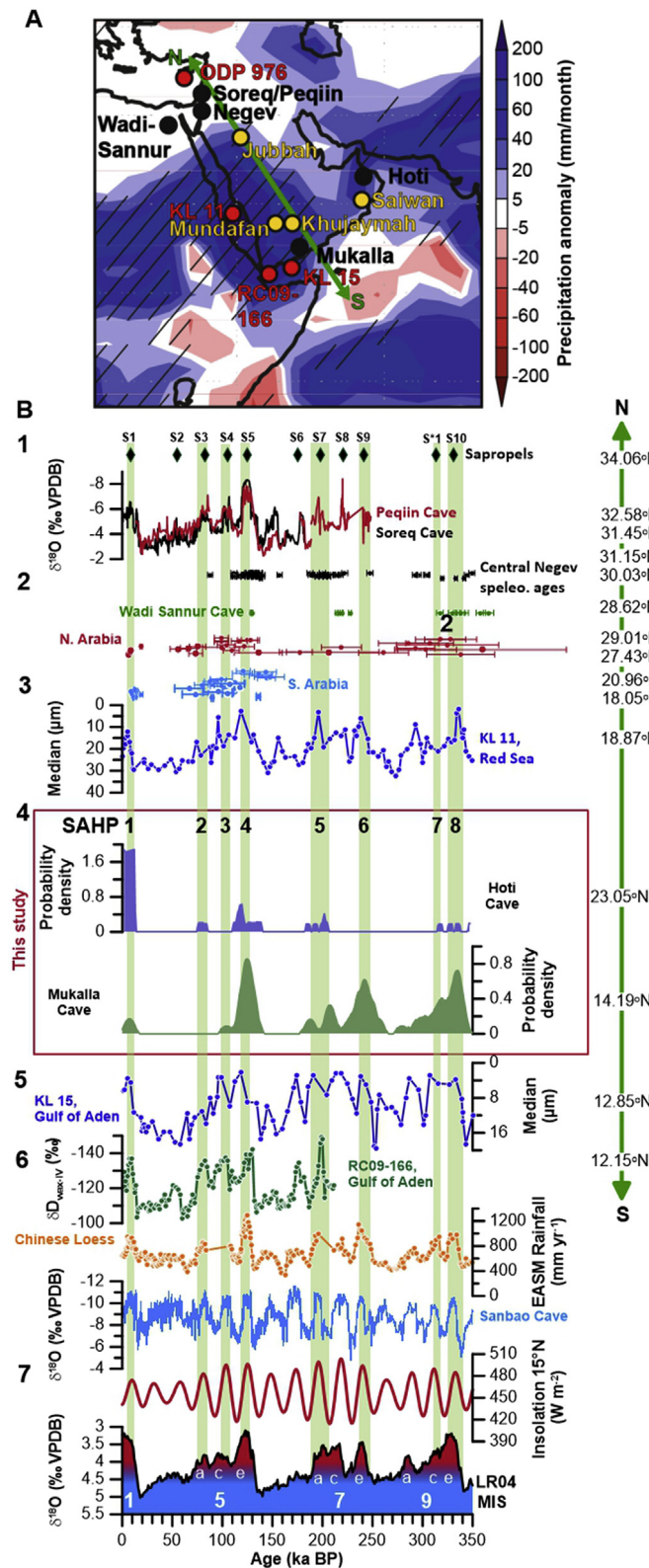


Fig. 4. (A) Location of speleothems (black circles), palaeolakes (yellow circles) and marine sediment cores from the eastern Saharo-Arabian deserts compared to simulated precipitation anomalies (MIS 5e – pre-industrial: Herold and Lohmann, 2009). (1) Sapropel layers in the Eastern Mediterranean Sea (green diamonds; Williams et al., 2015; Grant et al., 2017) vs Peqin Cave (red) and Soreq Cave (black; Bar-Matthews et al., 2003) $\delta^{18}\text{O}$ records; (2) central Negev (black; Vaks et al., 2010) and Wadi-Sannur (green; El-Shenawy et al., 2018) speleothem deposition periods compared to north (red; Petraglia et al., 2012; Rosenberg et al., 2013; Parton et al., 2018) and south Arabian

exception of SAHP 6 (~245–241 ka), in which there is only limited evidence of speleothem deposition (Vaks et al., 2010). Also, SAHPs 1–8 correlate to phases of lake formation in the Nafud desert in Northern Arabia related to enhanced ASM rainfall (Rosenberg et al., 2013; Jennings et al., 2015b). SAHPs are therefore in phase with wet intervals in Northern Arabia. One notable discrepancy, however, is the lack of evidence for stalagmite growth in Mukalla and Hoti Caves during MIS 7c (Fig. 4); whereas increased precipitation is observed in Wadi-Sannur Cave, Peqin and Soreq $\delta^{18}\text{O}_{\text{ca}}$ records, KL-15 grain size and Mediterranean sapropels (S8) (Fig. 4). MIS 7c is also reflected by a less substantial enhancement of the monsoon in Asia (Beck et al., 2018) and KL-11 (Fleitmann, 1997) (Fig. 4). The reason of lack of evidence for a SAHP during MIS 7c remains unknown. Furthermore, we acknowledge that some fluvio-lacustrine deposition and alluvial aggradation occurred in Arabia during MIS 6 and 3 (e.g., McLaren et al., 2009; Parton et al., 2013, 2015; 2018; Hoffmann et al., 2015). Previous analyses have shown that only 200 mm yr⁻¹ is required to activate alluvial systems in Arabia (Parton et al., 2015); whereas more than 300 mm yr⁻¹ is required to activate the growth of tall stalagmites (Vaks et al., 2010; Fleitmann et al., 2011).

The influence of precessional and glacial boundary forcing on Asian monsoon intensity remains controversial, as some monsoon records suggest dominant precession-driven monsoon maxima during Northern hemisphere summer insolation maxima (Cheng et al., 2016) while others show evidence for a dampening effect of glacial boundary conditions on monsoon strength during glacial periods (Burns et al., 2001; Fleitmann et al., 2003a; Beck et al., 2018). A recently published East Asian summer monsoon (EASM) reconstruction based on ^{10}Be -flux from Chinese loess shows highest summer monsoon rainfall during peak interglacial periods (Fig. 4). The ^{10}Be -flux rainfall EASM record is closely linked with global ice volume, which is consistent with the timing of SAHPs 1–8 in our speleothem record (Fig. 4).

In summary, there is excellent agreement between SAHPs and low latitude northern-hemisphere insolation, glacial boundary conditions and African and Asian (Indian) monsoon records. This adds confidence that the Mukalla and Hoti Cave speleothems are an accurate recorder of changes in ASM and ISM intensity and extent in north-eastern Africa and the Southern Arabian Peninsula.

4.1.3. Source of moisture in Southern Arabia during SAHPs 1 to 8

Current climate reconstructions derived from lacustrine sediments and dune deposits are unable to identify the source of precipitation during Arabian pluvial periods (Fleitmann et al., 2003b; Kutzbach et al., 2014; Enzel et al., 2015; Torfstein et al., 2015; Engel et al., 2017). This has triggered controversial debates about the origin of rainfall at the time of their formations. Enzel et al. (2015), for instance, questioned the paradigm that enhanced precipitation in Arabia was related to an amplification of the ASM and ISM and northward displacement of the summer ITCZ. Instead, Enzel et al. (2015) proposed two other potential sources of precipitation in Oman during the early and mid-Holocene humid period (SAHP 1): more frequent Arabian Sea cyclones or enhanced advection of moisture from the Gulf of Oman in winter. Direct measurements of

lakes (blue; Rosenberg et al., 2011, 2012; Matter et al., 2015); (3) Red Sea median grain size (Fleitmann, 1997); (4) age kernel density plots of Hoti Cave (blue; 5 pt moving average) and Mukalla Cave (green) stalagmites; (5) Gulf of Aden median grain size (Fleitmann, 1997) and $\delta D_{\text{leafwax}} (\text{‰})$ (Tierney et al., 2017); (6) Chinese reconstructed rainfall (Beck et al., 2018) vs Sanbao Cave composite speleothem $\delta^{18}\text{O}_{\text{ca}}$ record (Cheng et al., 2016); (7) Northern hemisphere June insolation at 15°N (Berger and Loutre, 1991, 1999) vs global marine $\delta^{18}\text{O}_{\text{benthic}}$ (Lisicki and Raymo, 2005). Marine Isotope Stages follow the taxonomy of Railsback et al. (2015). (For interpretation of the references to colour in this figure legend, the reader is referred to the Web version of this article.)

hydrogen and oxygen isotope values in speleothem fluid inclusions from Hoti and Mukalla Caves provide direct information on drip water isotopic composition and palaeoprecipitation respectively (Fleitmann et al., 2003b). Stalagmite δD_{FI} and $\delta^{18}\text{O}_{\text{FI}}$ values enable us to determine the origin (e.g., Mediterranean or Indian Ocean) and transport of moisture to Southern Arabia during pluvial periods. Furthermore, they also permit a direct comparison with isotope-enabled climate model simulations, to benchmark the models (Herold and Lohmann, 2009) and also help to settle current debates about the origin and seasonality of precipitation in Southern Arabia.

At present, a large proportion of moisture in Yemen derives from the northern reach of the ISM (Fleitmann et al., 2011) with additional moisture originating from Africa (by the ASM) and the Red Sea (mainly in winter/spring) (e.g., Al-ameri et al., 2014). The isotopic composition of modern precipitation (collected between 2008 and 2010) from sampling sites between 500 and 1700 m asl in Yemen ranges from around -40 to $40\text{\textperthousand}$ and -4 to 8\textperthousand in δD and $\delta^{18}\text{O}$ respectively, and rainfall plots along the Global Meteoric Waterline (GMWL; $\delta D = 8 \delta^{18}\text{O} + 10$; Fig. 5A; Al-ameri et al., 2014). In contrast, stalagmite Y99 fluid inclusion isotope values for MISs 5e (SAHP 4) and 7e (SAHP 6) are more negative and range from $-64.5\text{\textperthousand}$ to $-35.0\text{\textperthousand}$ and -8.6 and $-4.5\text{\textperthousand}$ in δD and $\delta^{18}\text{O}$ respectively (Fig. 5A; Table S9). Like modern rainfall, Y99 fluid inclusion isotope values plot close to the GMWL, whereas some samples appear to be slightly affected by evaporation as they plot below the GMWL. Stalagmite Y99 MIS 5e and MIS 7e δD_{FI} and $\delta^{18}\text{O}_{\text{FI}}$ values are more negative than isotope values in modern summer monsoonal rainfall (June to September) in Addis Ababa, Ethiopia, where moisture is delivered by the African and Indian summer monsoons. This suggests that enhanced rainfall at Mukalla Cave during MIS 5e (SAHP 4) and MIS 7e (SAHP 6) resulted from an amplification of the ASM and/or ISM (Fig. 5C). Our assumption is also supported by climate model data for MIS 5e (Herold and Lohmann, 2009; Jennings et al., 2015b), which indicate a more zonal transport of moisture from Africa to the Arabian Peninsula during MIS 5e (SAHP 4). Y99 $\delta^{18}\text{O}_{\text{FI}}$ values of around $-7.2 \pm 1.5\text{\textperthousand}$ during MIS 5e are within the range of modelled summer precipitation $\delta^{18}\text{O}$ values of between -6 and $-7\text{\textperthousand}$ in Yemen (Fig. 5C). Finally, significant contributions of rainfall from a Mediterranean source can be excluded as Y99 δD_{FI} and $\delta^{18}\text{O}_{\text{FI}}$ values plot below the Mediterranean Meteoric Waterline (MMWL; $\delta D = \delta^{18}\text{O} + 22$; Fig. 5A).

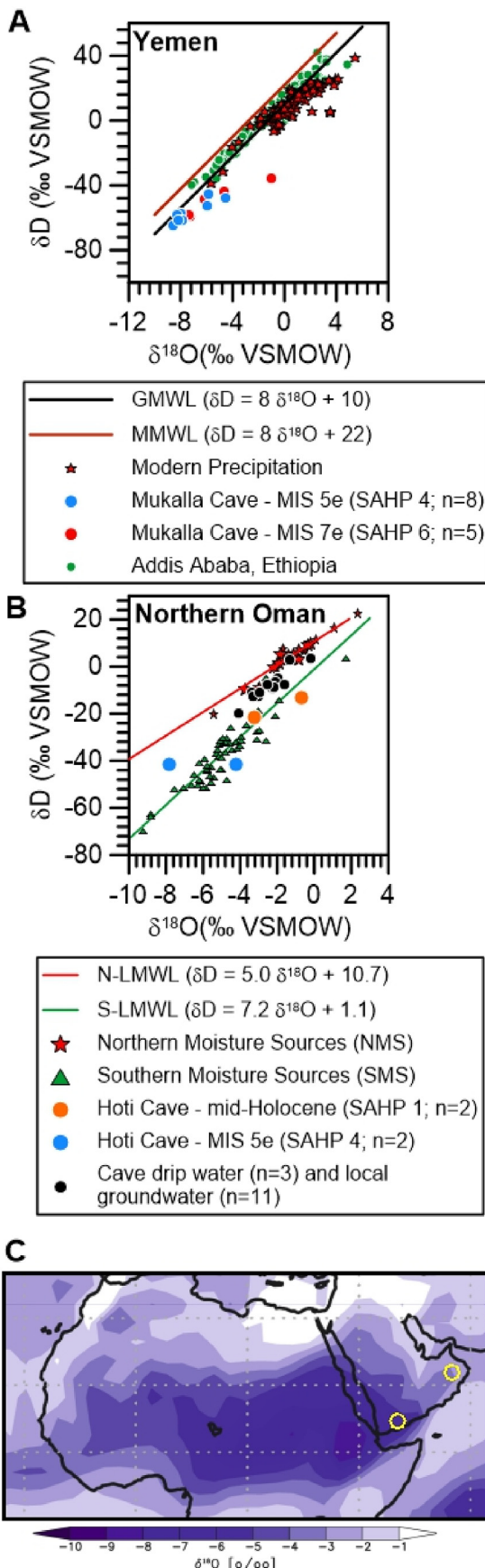
In Northern Oman, present-day rainfall originates predominantly from a northern (Mediterranean) and a southern (Indian Ocean) moisture source. As a result, two distinctly different local meteoric waterlines exist, the Northern Meteoric Waterline (N-LMWL; $\delta D = 5.0 \delta^{18}\text{O} + 10.7$) and the Southern Local Meteoric Waterline (S-LMWL; $\delta D = 7.1 \delta^{18}\text{O} - 1.1$) (Fig. 5B; Weyhenmeyer et al., 2002; Fleitmann et al., 2003b). Precipitation originating from a northern moisture source ranges from -4.5 to $1.0\text{\textperthousand}$ in $\delta^{18}\text{O}$ and from -25 to 5\textperthousand in δD , whereas precipitation from a southern moisture source is more negative, with $\delta^{18}\text{O}$ values varying from -10 to $-2\text{\textperthousand}$ and δD values from -75 to $-15\text{\textperthousand}$ (Weyhenmeyer et al., 2002; Fleitmann et al., 2003b). Modern groundwater in Northern Oman (N-OGL; $\delta D = 5.3 \delta^{18}\text{O} + 2.7$) and cave drip water in Hoti Cave is intermediate between both sources, indicating that both contribute to groundwater recharge (Weyhenmeyer et al., 2002; Fleitmann et al., 2003b, Fig. 5B). The isotopic composition of fluid inclusion water extracted from the Holocene stalagmite H5 (SAHP 1: 10.9 ka–6.2 ka; Neff et al., 2001; Fleitmann et al., 2007) ranges from $-21.4\text{\textperthousand}$ to $-13.2\text{\textperthousand}$ in δD_{FI} , and $-3.2\text{\textperthousand}$ to $-0.7\text{\textperthousand}$ in $\delta^{18}\text{O}_{\text{FI}}$. Fluid inclusion water extracted from the MIS 5e (SAHP 4) section of stalagmite H13 is more negative and measured $-41.7\text{\textperthousand}$ for δD_{FI} and $-7.8\text{\textperthousand}$ to $-4.2\text{\textperthousand}$ for $\delta^{18}\text{O}_{\text{FI}}$. Both H5 and H13 fluid

inclusion values plot closer to the S-LMWL (Fig. 5B), indicating the ISM was the primary moisture source in Oman during peak interglacials (Fleitmann et al., 2003b). One sample, however, plots above the S-LMWL, yet this remains more closely aligned to modern southern groundwater values. Overall, Hoti Cave δD_{FI} and $\delta^{18}\text{O}_{\text{FI}}$ values show clear evidence that enhanced rainfall during the early to middle Holocene (SAHP 1) and MIS 5e (SAHP 4) was related to an intensification of the ISM. This is in stark contrast to suggestions that enhanced frontal depressions from the Persian Gulf and/or Mediterranean increased precipitation during the early to mid-Holocene wet period (SAHP 1) (Enzel et al., 2015).

When compared to isotope-enabled climate model simulation, the measured isotope $\delta^{18}\text{O}_{\text{FI}}$ values at both caves for SAHP 4 (MIS 5e) are in good agreement with modelled $\delta^{18}\text{O}$ of summer precipitation (Fig. 5C). Furthermore, the distinct isotopic gradient across Southern Arabia is also supported by the Y99 and H13 $\delta^{18}\text{O}_{\text{FI}}$ values, with more negative modelled summer rainfall $\delta^{18}\text{O}$ values prevailing in the west due to a greater moisture supply from the African summer monsoon (Herold and Lohmann, 2009). Thus, growth intervals and isotope values in stalagmites from Mukalla Cave are excellent proxies for the intensity of the ASM in eastern Africa, whereas stalagmites from Hoti Cave are more closely connected to intensity changes of the ISM and, to a lesser extent, ASM. This is also in agreement with climate model simulations for MIS 5e, which indicate that higher precipitation in Northern Oman was associated with the ASM and ISM, with negligible and fairly stable contribution of rainfall from Mediterranean westerlies (Jennings et al., 2015b).

4.1.4. Comparison between pluvial conditions in Southern Arabia during the last 350 ka

$\delta^{18}\text{O}_{\text{ca}}$ values of stalagmites from Southern Arabia are primarily controlled by two effects: i.e. the amount and source of rainfall (Fleitmann et al., 2003b, 2004, 2007, 2011). $\delta^{18}\text{O}_{\text{ca}}$ values of Mukalla Cave stalagmites are generally more negative than those of stalagmites from Hoti Cave (Fig. 6A), with a west-east (Mukalla-Hoti) isotopic gradient of between 2 and 4\textperthousand during SAHPs 1–7. This gradient is also evident in δD_{FI} and $\delta^{18}\text{O}_{\text{FI}}$ values from both caves and in simulated MIS 5e $\delta^{18}\text{O}$ in summer precipitation across Southern Arabia (Fig. 5). This adds further confidence in the palaeoclimatic significance of $\delta^{18}\text{O}_{\text{ca}}$ values from Mukalla and Hoti Caves. Furthermore, $\delta^{18}\text{O}_{\text{ca}}$ values from both cave sites reveal marked and consistent differences in the amount of rainfall between among the SAHPs (Fig. 6A). The most striking feature of the Mukalla and Hoti Cave records is the fact that least negative $\delta^{18}\text{O}_{\text{ca}}$ values were obtained from early to mid-Holocene stalagmites, indicating that monsoon rainfall during SAHP 1 was the lowest in the last 350 ka. On the other hand, monsoon precipitation was highest at both caves during SAHP 4 (MIS 5e). When we combine our fluid inclusion data with the relatively consistent $\delta^{18}\text{O}_{\text{ca}}$ between SAHPs, we can show that the moisture source was likely consistent throughout SAHPs. Modern $\delta^{18}\text{O}_{\text{ca}}$ values from Hoti Cave (derived from the winter Mediterranean precipitation source) are more positive than SAHP values (Fig. 6A). SAHP 1 (early to middle Holocene), 4 (MIS 5e) and 6 (MIS 7e) FI data allows us to confidently state that $\delta^{18}\text{O}_{\text{ca}}$ of these periods represents a monsoon rainfall signature. Thus, we can use the more positive $\delta^{18}\text{O}_{\text{ca}}$ values (Mediterranean signature) of modern and more negative $\delta^{18}\text{O}_{\text{ca}}$ values (monsoon signature) of past precipitation to posit that monsoon precipitation was the dominant source of preceding SAHPs. This isotopic relationship has also been observed in previously published high-resolution $\delta^{18}\text{O}_{\text{ca}}$ profiles of H5 and H12 (Fig. 6B), where an abrupt shift from more negative values (increased precipitation from the ISM) to more positive values (reduced precipitation delivered by Winter Mediterranean Cyclones (WMCs)) occurred at



the termination of the early Holocene pluvial period (SAHP 1) (Fleitmann et al., 2007).

4.1.5. Environmental conditions

Mukalla Cave speleothem $\delta^{13}\text{C}_{\text{ca}}$ values vary between -8 and 2\textperthousand (VPDB) (Fig. 7; Table S11). Such a wide range in $\delta^{13}\text{C}_{\text{ca}}$ is quite common in speleothems as $\delta^{13}\text{C}_{\text{ca}}$ depends on a variety of environmental, partly counteracting, parameters, including: (1) type and density of vegetation, (2) soil thickness and moisture, (3) biological activity within the soil, (4) recharge conditions and (5) kinetic isotope fractionation during calcite precipitation, the latter factor is influenced by cave air PCO_2 and drip rate (e.g., Baker et al., 1997). At times of high precipitation and short soil-water residence times, equilibration between soil CO_2 and percolating water may be incomplete. Under such a scenario, seepage water would have a stronger atmospheric CO_2 component and thus speleothem $\delta^{13}\text{C}_{\text{ca}}$ values would be more positive. In addition, CO_2 degassing within the cave can lead to more positive speleothem $\delta^{13}\text{C}_{\text{ca}}$ values and thus blur the biogenic signal. Overall, speleothem $\delta^{13}\text{C}_{\text{ca}}$ values can be difficult to interpret, which is one reason why the Hoti Cave $\delta^{13}\text{C}_{\text{ca}}$ records were never used for palaeoenvironmental reconstructions. This is also related to the fact that Hoti Cave has two entrances and therefore strong ventilation, leading to fluctuations in cave air PCO_2 and strong kinetic fractionation of $\delta^{13}\text{C}$ during calcite precipitation. In contrast, Mukalla Cave has only one narrow entrance and ventilation within the cave is therefore low. Mukalla Cave stalagmite $\delta^{13}\text{C}_{\text{ca}}$ values are therefore more closely related to surface vegetation and biological soil activity, provided that complete equilibration ("open system conditions") between soil CO_2 and soil water has occurred. Under such conditions, $\delta^{13}\text{C}_{\text{ca}}$ values of a stalagmite growing under a C_3 plant dominated environment vary between -14 and $-6\text{\textperthousand}$ (VPDB) and -6 to $+2\text{\textperthousand}$ under C_4 plants (Clark and Fritz, 1997; McDermott, 2004). Assuming open system conditions, Mukalla Cave speleothem $\delta^{13}\text{C}_{\text{ca}}$ values fall into the range of C_4 plant dominated vegetation with occasional C_3 plants (Fig. 7), indicating herbaceous semi-desert grassland environment above the cave during SAHPs 1–8.

Our data also shows that C_4 environments were present during the warm substages of MIS 5. This is in good coherence with phytolith data from the Jabal Faya archaeological site, UAE, showing denser and more diverse vegetation was present during MIS 5 than succeeding substages (Bretzke et al., 2013). Grassland taxa (*Kobus*, *Hippopotamus*, *Pelovoris*) and *H. sapiens* were uncovered from MIS 5a palaeolake sediments in the Nafud showing that grasslands were present in northern Arabia (Groucutt et al., 2018). In particular, *Hippopotamus* is not a long-distance migratory species, and requires year-round access to water. Similarly, the MIS 5e speleothem $\delta^{13}\text{C}_{\text{ca}}$ values from Ashhalim Cave, Negev, range from $-8\text{\textperthousand}$ to $-2\text{\textperthousand}$ (Vaks et al., 2010), suggesting comparable environments existed in the northern and southern extent of the Saharo-Arabian

Fig. 5. Water isotope (δD_{FI} and $\delta^{18}\text{O}_{\text{FI}}$) values from stalagmites from Mukalla and Hoti Caves (Table S9). (A) Stalagmite Y99 δD_{FI} and $\delta^{18}\text{O}_{\text{FI}}$ values in comparison to δD and $\delta^{18}\text{O}$ in modern precipitation in Yemen (Al-ameri et al., 2014) and Ethiopia (IAEA/WMO, 2019). Global Network of Isotopes in Precipitation, The GNIP Database. Accessible at: <https://nucleus.iaea.org/wiser>. Black line denotes the Global Meteoric Waterline (G-MWL: $\delta D = 8 \delta^{18}\text{O} + 10$). Brown line denotes the Mediterranean Meteoric Waterline ($\delta D = 8 \delta^{18}\text{O} + 22$) (Gat and Carmi, 1970; Matthews et al., 2000; McGarry et al., 2004). (B) δD_{FI} and $\delta^{18}\text{O}_{\text{FI}}$ values H5 and H13 compared to regional precipitation values and meteoric waterlines from Northern Oman (N-LMWL: $\delta D = 5.0 \delta^{18}\text{O} + 10.7$; Weyhenmeyer et al., 2000, 2002) and Southern Oman (S-LMWL: $\delta D = 7.2 \delta^{18}\text{O} + 1.1$; Weyhenmeyer et al., 2000, 2002). (C) Locations of Mukalla Cave and Hoti Cave relative to modelled $\delta^{18}\text{O}_{\text{precipitation}}$ values for boreal summer precipitation during MIS 5e (modified after Herold and Lohmann, 2009). Yellow circles mark the location of Mukalla and Hoti Caves. (For interpretation of the references to colour in this figure legend, the reader is referred to the Web version of this article.)

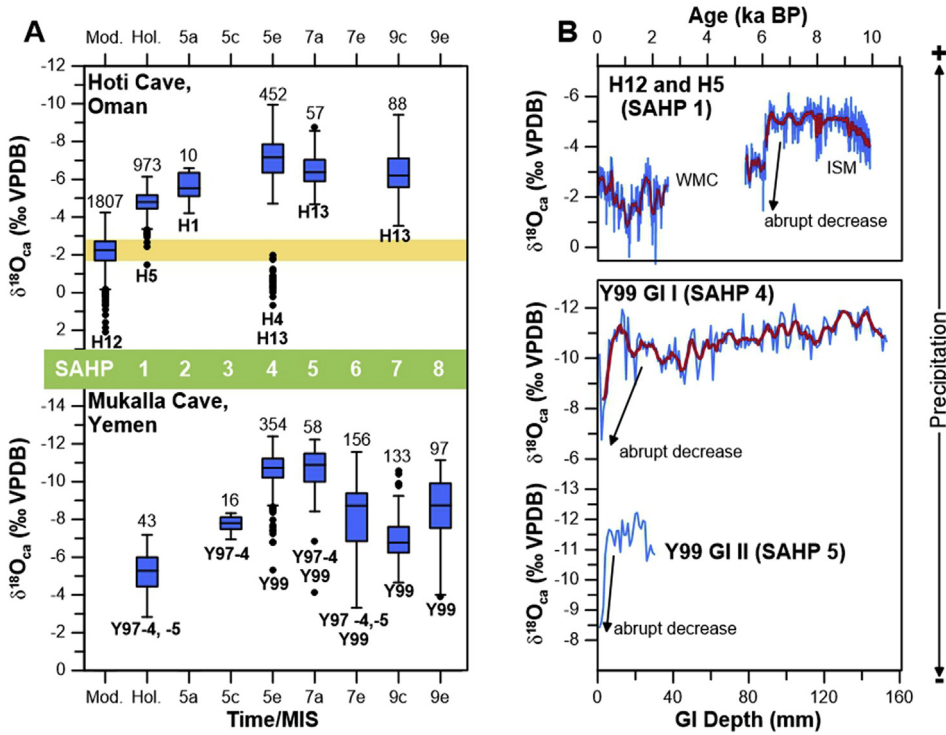


Fig. 6. (A) $\delta^{18}\text{O}_{\text{ca}}$ whisker-boxplot of Mukalla Cave and Hoti Cave composite records (new Y99 $\delta^{18}\text{O}_{\text{ca}}$ values combined with data from Fleitmann et al., 2011; Table S10). Numbers below whiskers denote sample labels and number of $\delta^{18}\text{O}_{\text{ca}}$ measurements. Statistically extreme values marked as black circles. (B) $\delta^{18}\text{O}_{\text{ca}}$ profiles of Holocene (H5 and H12), MIS 5e (Y99 GI I) and MIS 7a (Y99 GI II) stalagmites.

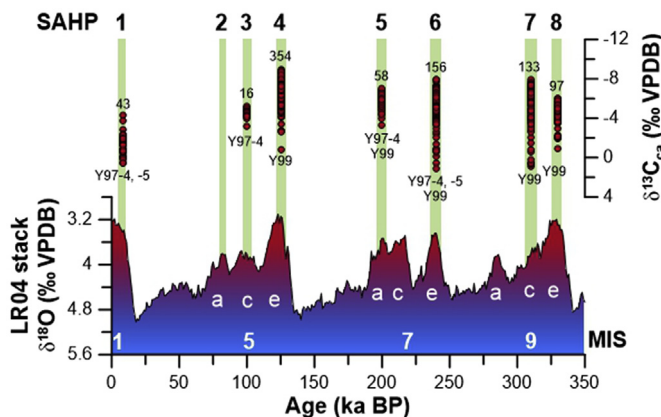


Fig. 7. $\delta^{13}\text{C}_{\text{ca}}$ values of Mukalla Cave speleothems during SAHPs I-V (Table S11) compared to the LR04 stack $\delta^{18}\text{O}$ record (Lisicki and Raymo, 2005).

desert. Archaeological and fossils finds have demonstrated that *H. sapiens* were present in Arabia during MIS 5 interstadials (Groucett et al., 2018). Furthermore, Mukalla Cave $\delta^{13}\text{C}_{\text{ca}}$ values are coherent with palaeontological evidences from older pluvial periods. Faunal assemblages from the Ti's al Ghadah palaeolake (MIS 9–13) exhibit large mammals from African and European sources (Thomas et al., 1998; Rosenberg et al., 2013; Stimpson et al., 2016), showing these wet periods were sufficient to sustain fauna that required a perennial water supply. Overall, our data adds to the growing evidence that the formation of widespread 'green' environments formed across Arabia during peak interglacial periods, which facilitated *H. sapiens* occupation and movement across the now desert areas of Arabia.

4.1.6. Seasonality of precipitation during SAHPs

Some stalagmites from Hoti Cave exhibit distinct annual layers, with a thickness varying between 0.1 and 1.2 mm (e.g., stalagmite H14; Cheng et al., 2009). Such layers are also visible in the MIS 5e section of stalagmite H13, composed of a white porous laminae and dense translucent laminae. Their presence suggests distinct seasonal changes in the drip rate in response to surface precipitation. Nearly monthly resolved $\delta^{18}\text{O}_{\text{ca}}$ and $\delta^{13}\text{C}_{\text{ca}}$ profiles over 4 years (Fig. 8B; Table S8) show seasonal variations of more than 1‰, where denser layers display more negative $\delta^{18}\text{O}_{\text{ca}}$ and $\delta^{13}\text{C}_{\text{ca}}$ values. We suggest that these denser layers were formed during the monsoon seasons, at times of higher drip rate, slower CO₂ degassing and lower evaporation of cave drip waters (Fleitmann et al., 2004). In contrast, the more porous white layers display more positive $\delta^{18}\text{O}_{\text{ca}}$ and $\delta^{13}\text{C}_{\text{ca}}$ due to a reduced drip rate, resulting in greater CO₂ degassing and evaporation. Combined with δD_{FI} and $\delta^{18}\text{O}_{\text{FI}}$ values from H13, the presence of annual layers during SAHP 1 (early to mid-Holocene; Cheng et al., 2009) and SAHP 4 (MIS 5e; this study) and seasonal changes in $\delta^{18}\text{O}_{\text{ca}}$ and $\delta^{13}\text{C}_{\text{ca}}$ indicates that Southern Arabia experienced a rainy (monsoon) season during boreal summer and a drier season during boreal winter. This is in good agreement with climate simulations for MIS 5e, with simulations at 130, 125 and 120 ka BP (Gierz et al., 2017). These simulations show a strong increase in summer (JJA) precipitation at 130 and 125 ka BP, whereas no significant increase in winter (DJF) is observed in Southern Arabia (Fig. 8C). We can therefore exclude that increased precipitation was provided by enhanced Mediterranean cyclone activity in winter/spring as suggested Enzel et al. (2015). Taken together, there is clear evidence that climatic conditions during SAHPs were still characterized by a strong seasonality with wet summers and rather dry winters.

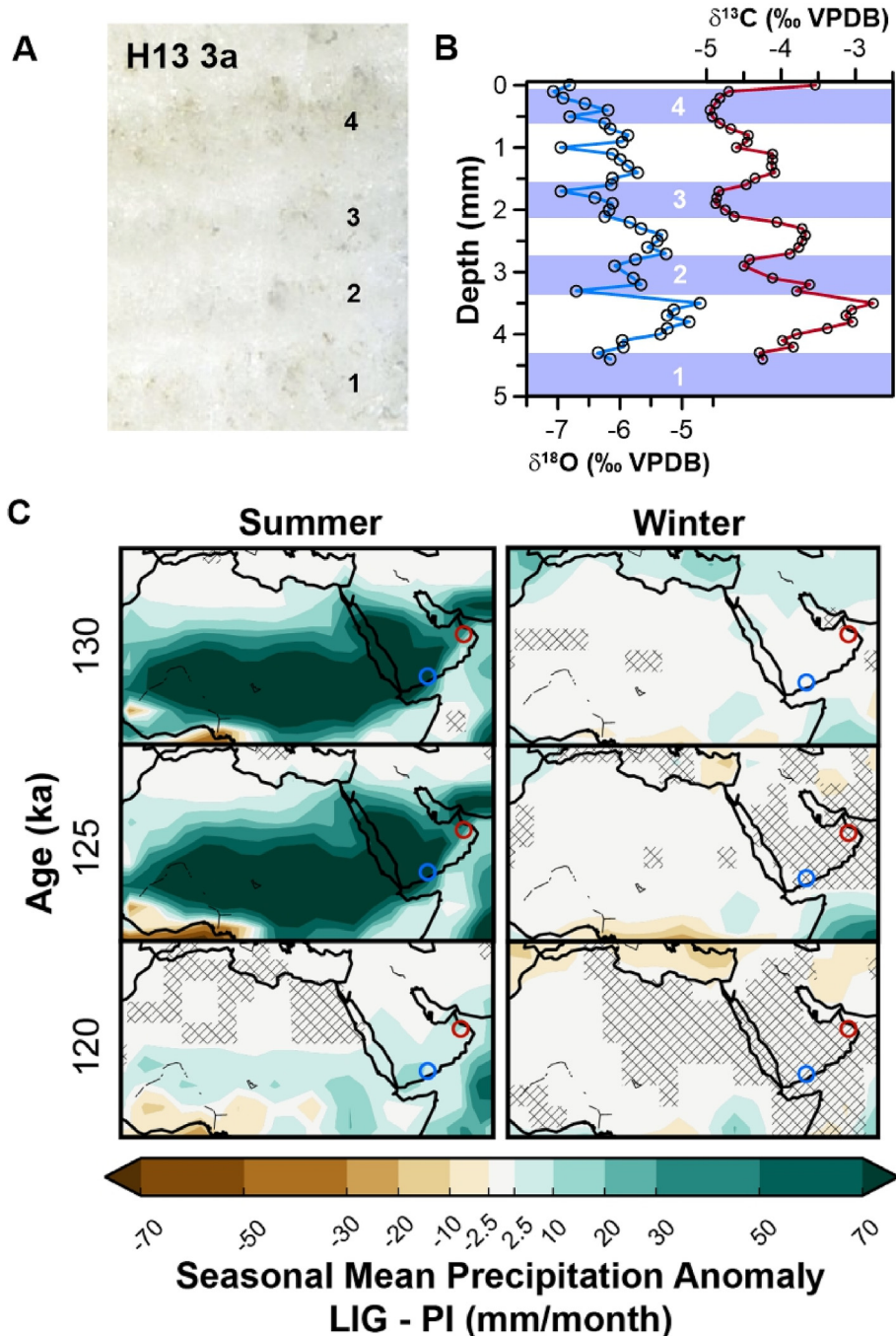


Fig. 8. (B) Sub-annual $\delta^{18}\text{O}_{\text{ca}}$ and $\delta^{13}\text{C}_{\text{ca}}$ values from a MIS 5e section of stalagmite H13 (A) from Hoti Cave (Table S8). Shaded blue areas and numbers mark the monsoon seasons. (C) Mukalla Cave (blue circle) and Hoti Cave (red circle) mapped to modelled MIS 5e winter and summer precipitation anomaly (compared to pre-industrial) (Gierz et al., 2017). (For interpretation of the references to colour in this figure legend, the reader is referred to the Web version of this article.)

4.2. Timing and nature of SAHPs beyond 350 ka

4.2.1. Chronology of stalagmite Y99 beyond 350 ka

The identification of Y99 GIs beyond 350 ka BP is based (1) on thirty-one ^{230}Th and three U-Pb ages (Tab. S1, S2 and S4), (2) macroscopic evidence for major discontinuities (e.g., abrupt changes in colour of the fabric, abrupt changes in the frequency of laminae, finely defined and bright laminae and lateral displacements of the growth axis), and (3) abrupt shifts in $\delta^{18}\text{O}_{\text{ca}}$ over potential discontinuities (Fig. 2D). The latter are strong evidence for

the termination of a SAHP, as they occur immediately before the cessation of stalagmite growth, when annual precipitation dropped below 300 mm yr^{-1} (Burns et al., 2001; Fleitmann et al., 2003b). Positive shifts in $\delta^{18}\text{O}_{\text{ca}}$ are also observed in stalagmites from Hoti Cave, where they mark a weakening and termination of pluvial monsoon periods within a few decades. This is particularly evident ~6.2 ka BP (Neff et al., 2001; Fleitmann et al., 2007, Fig. 6B). Using these criteria, we identified 12 further GIs (VI to XVIII) in stalagmite Y99. However, it is slightly more challenging to assign absolute ages to these GIs, as it becomes increasingly difficult to obtain accurate

and precise ^{230}Th ages beyond 400 ka BP. While the chronology of Y99 Glaciers VI–XVIII is supported by thirty-one ^{230}Th and three U-Pb ages, ^{230}Th ages for Glaciers VI to VIII are not in perfect stratigraphic order, with several age reversals occurring between 400 and 550 ka BP. This is not related to analytical problems but rather caused by post-depositional mobilisation of U and Th, potential small-scale dissolution and re-precipitation of calcite or incorporation of ^{230}Th adsorbed to organic acids (Borsato et al., 2003; Scholz et al., 2014). These effects can imply localized open-system behaviour (Bajo et al., 2016). While post-depositional leaching of U would lead to older ages, re-precipitation of calcite or incorporation of ^{230}Th would result in younger ages as observed in some Glaciers. All these effects are critical for very old samples that are close to the ^{230}Th -dating limit of ~500–600 ka as even minute post-depositional alterations and several phases of dissolution and/or re-precipitation can have significant effects on the age. The higher porosity and micro-voids make the upper section of stalagmite Y99 (Fig. 2A and B) more prone to post-depositional loss or addition of radionuclides. In contrast, the lower part of Y99, comprising Glaciers IX to XVIII, is composed of very dense calcite but too old for the ^{230}Th -dating method. Nevertheless, two U-Pb ages determined in different laboratories are consistent and date the base of stalagmite Y99 to 1.07 ± 0.04 Ma (GI XVIII; MIS 31). One additional U-Pb age of 0.85 ± 0.07 Ma BP for GI XII serves as an additional tie point for the chronology of the lower part of stalagmite Y99. Based on the consistent pattern of high-monsoonal rainfall and stalagmite growth during interglacial intervals during the last 350 ka BP (Fig. 4), we used orbital tuning to the LR04 stack (Lisicki and Raymo, 2005) to assign absolute ages for Y99 Glaciers VI to XIII and XIV to XVII (Fig. 9). The good match between the number of identified Glaciers and peak interglacial periods gives credence to the Y99 chronology.

4.2.2. Climate and environmental conditions in Southern Arabia over the last 1.1 Ma

At least 21 SAHPs occurred over the last 1.1 Ma at times when low ice volume and high summer insolation strengthened both the

ISM and ASM. As mentioned previously, there is a general scarcity of terrestrial records covering more than 400 to 500 ka BP in Northern Africa and the Arabian Peninsula, and marine sediments are the only source of information. Two dust records from the Eastern Mediterranean (ODP 967; Grant et al., 2017) and Arabian Sea (ODP 721/722; deMenocal, 1995) extend beyond 500 ka BP and are interpreted to reflect continental wetness in the wider north-east African region and the Arabian Peninsula (Fig. 10). The ODP 967 PCA index of rainfall and aridity (PC2; Fig. 10) is based on trace element content (e.g., titanium) and sapropels and shows distinct fluctuations in the strength and spatial extent of the ASM. The ODP 967 record thus provides evidence for multiple “Green Sahara Periods”. When compared to the stalagmite record of SAHPs, some wet periods in the ODP 967 record coincide with SAHPs, such as during the early to middle Holocene, MIS 5e, 7a, 9e and 13a (Fig. 10). There are also notable differences and wet climatic phases in the ODP 967 PC2 record are not always consistent with SAHPs, such as MIS 6 or MIS 16. Adversely, between 950–650 ka BP, the ODP 967 rainfall index is typically in a ‘dry’ mode while at least three SAHPs occurred within MIS 17, 19 and 21. Likewise, the association between SAHPs and low dust content in the ODP 721/722 core is not always evident. For instance, dust content is relatively low and constant between MISs 12 and 16, suggesting rather humid climatic conditions between 425 and 675 ka BP. The discrepancy between dust and stalagmite records has been observed before (Fleitmann et al., 2011) and could be related to regional variability, availability of dust and changes in wind direction and strength.

Stalagmite Y99 $\delta^{18}\text{O}_{\text{ca}}$ values of all Glaciers are very similar and typically range from -7 to $-11\text{\textperthousand}$ (Fig. 9), indicating that the ASM was the dominant source of precipitation during all SAHPs. There are, however, differences in the degree of wetness between SAHPs as more negative $\delta^{18}\text{O}_{\text{ca}}$ values indicate higher ASM and ISM rainfall in Yemen and Oman. The boxplot (Fig. 9) of $\delta^{18}\text{O}_{\text{ca}}$ values of all Mukalla Cave stalagmites show that SAHPs 4, 5, 18, 19 and 20 exhibit the most negative $\delta^{18}\text{O}_{\text{ca}}$ values and are thus characterized by the highest monsoonal rainfall.

Y99 $\delta^{13}\text{C}_{\text{ca}}$ values range 2 to $-8\text{\textperthousand}$ (Fig. 9) and differences are

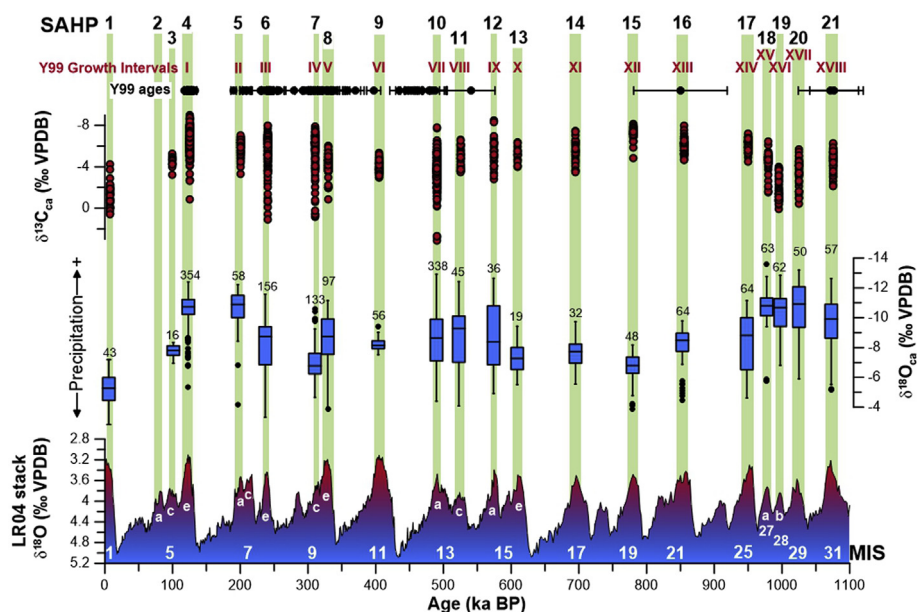


Fig. 9. ^{230}Th (Tables S1–S3) and U-Pb (Tables S4 and S5) ages for stalagmite Y99 compared to the LR04 stack $\delta^{18}\text{O}$ record (Lisicki and Raymo, 2005) and extended $\delta^{18}\text{O}_{\text{ca}}$ and $\delta^{13}\text{C}_{\text{ca}}$ records of Mukalla Cave stalagmites (Y97–4, Y97–5 and Y99). Undated Y99 growth intervals were assigned to intermediate interglacials and warm substages. Green bars denote timing of SAHPs (South Arabian Humid Periods). Marine Isotope Stages follow the taxonomy of Railsback et al. (2015). (For interpretation of the references to colour in this figure legend, the reader is referred to the Web version of this article.)

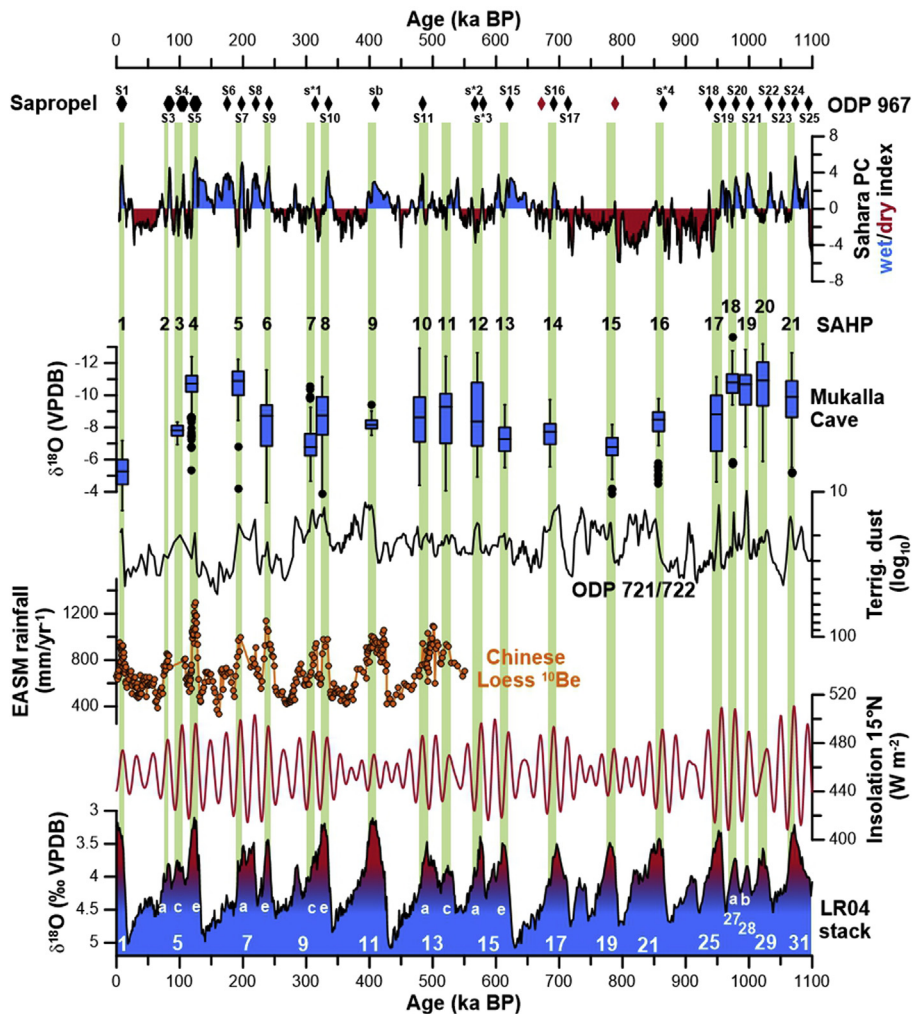


Fig. 10. SAHPs (green bars) and palaeoclimate records. (Eastern Mediterranean) ODP 967 sapropels (black = identified, red = 'ghost') and wet/dry PCA model (Grant et al., 2017); central Negev desert speleothem ages (Vaks et al., 2010); northern and Southern Arabian palaeolake ages (Rosenberg et al., 2011, 2012, 2013; Matter et al., 2015; Parton et al., 2018) and Mukalla Cave $\delta^{18}\text{O}_{\text{ca}}$ values; ODP 721/722 terrigenous dust (deMenocal, 1995); EASM reconstructed rainfall from Chinese $^{10}\text{Be}_{\text{loess}}$ (Beck et al., 2018); NHI insolation (W m^{-2}) at 15°N (Berger and Loutre, 1991, 1999) and LR04 stack foraminifera $\delta^{18}\text{O}_{\text{benthic}}$ (Lisiecki and Raymo, 2005) and Marine Isotope Stages following the taxonomy of Railsback et al. (2015). (For interpretation of the references to colour in this figure legend, the reader is referred to the Web version of this article.)

apparent between SAHPs. As stated above, these ranges are typical of C₄ environments above the cave assuming 'open system' conditions. However, $\delta^{13}\text{C}_{\text{ca}}$ values can be influenced by various parameters such as vegetation type and density, soil thickness and moisture, as well as atmospheric and other processes (McDermott, 2004; Rowe et al., 2012). Moreover, deluge of thin soils at times of very high rainfall can lead to more positive speleothem $\delta^{13}\text{C}_{\text{ca}}$ values due to rapid infiltration into the karst system and reduced interaction with soil CO₂ (e.g., Bar-Matthews et al., 2003). Increased rainfall during SAHP 19–20 could have led to more positive $\delta^{13}\text{C}_{\text{ca}}$ values. In contrast, reduced rainfall and increased interaction of percolating water with soil CO₂ may have had the opposite effect, contributing to more negative $\delta^{13}\text{C}_{\text{ca}}$ values during SAHP 14–17. Due to the numerous controls on speleothem $\delta^{13}\text{C}_{\text{ca}}$, alterations of the principal determinant can be expected over such a long period of time. Despite this, the overall range of $\delta^{13}\text{C}_{\text{ca}}$ values indicates C₄ grasslands were present during SAHP VI–XVII. This shows that interglacial periods routinely saw vegetation form in the now desert areas of southwestern Arabia.

4.3. Hominin migrations

4.3.1. Early–Middle Pleistocene

Estimates for the potential timing of hominin dispersals during the last few hundred thousand years are mostly modelled on palaeoclimate conditions of East Africa (deMenocal, 1995; Shultz and Maslin, 2013; Maslin et al., 2014) or Eurasia (Muttoni et al., 2010; Kahlke et al., 2011). These models do not consider whether and when the Saharo-Arabian desert was traversable. Yet the formation of so called "green corridors" between sub-Saharan Africa, northern Africa and Eurasia created "windows of opportunity" that would have been critical for hominin occupation and dispersal. Though, it is surely more apt to consider these areas as "green landscapes" in which hominin populations inhabited – rather than a route to the 'other' side. Based on the timing of SAHPs and their close connection to humid intervals in Northern Africa, we suggest that the Saharo-Arabian grasslands could facilitate occupation and dispersal during MIS 31 (~1080 ka: SAHP 21), MIS 29 (~1014 ka: SAHP 20), MIS 28b (~1000 ka: SAHP 19) MIS 27a (~982 ka: SAHP 18) MIS 25 (~955 ka: SAHP 17), MIS 21 (~850 ka: SAHP 16) and MIS 19 (~760 ka: SAHP 15) (Fig. 10). Frequent windows of opportunity took

place between SAHP 21 to SAHP 17 (MIS 31 to MIS 25), varying between 40–10 ka intervals. SAHP 21 to 18 are also marked as some of the most negative $\delta^{18}\text{O}_{\text{ca}}$ values in Y99 (Fig. 10), indicating intense monsoon periods. Succeeding this, SAHPs reduced in frequency, with ~100–70 ka intervals between SAHPs 17–13 (MIS 25–15e). These are also marked by increased $\delta^{18}\text{O}_{\text{ca}}$ values – indicating somewhat drier periods – and reduced occurrence of Mediterranean sapropels (Fig. 10). This shift echoes the transition from ~40 ka to ~100 ka glacial interglacial cycles, known as the Middle Pleistocene Transition (MPT) (Lisiecki and Raymo, 2005; Railsback et al., 2015; Tzedakis et al., 2017). Thus, it is likely that the pattern of hominin occupation of Arabia shifted in line with this transition, with longer gaps between occupations phases. However, we must emphasise that direct ages have not been attained for SAHPs 20–17 and 19–13, meaning this argument is currently somewhat tentative. Attaining direct ages for these SAHPs should be a target of future analysis.

The early appearance of *H. heidelbergensis* at Melka Kunture (Ethiopia) soon after ~875 ± 10 ka (MIS 21; Profico et al., 2016) and subsequent appearances in Eurasia is a key event in Early-Middle Pleistocene hominin evolution. SAHPs within this period provide potential timings for *H. heidelbergensis* dispersal, assuming an African origin for this species. While there is a paucity of absolute dating, Oldowan and Acheulean tool typologies have been uncovered in Southern Arabia (Chauhan, 2009; Groucutt and Petraglia, 2012 and references therein; Bailey et al., 2015; Bretzke et al., 2016). This suggests an additional behavioural adaptation was not required for Mode-1 or Mode-2 bearing hominins to occupy Arabia, at least as represented by the lithic record, but occupation was likely dependent on periods of ameliorated climatic conditions. Here, we have provided timings in which the Arabian Peninsula was occupiable and traversable.

SAHPs during MIS 17 (~700 ka: SAHP 14), MIS 15e (~600 ka: SAHP 13), MIS 15a (~675 ka: SAHP 12), MIS 13c (~530 ka: SAHP 11) and MIS 13a (~480 ka: SAHP 10) may have facilitated dispersals from Africa. Y99 $\delta^{18}\text{O}_{\text{ca}}$ have positive (SAHP 14 and 13) and variable (SAHP 12, 11 and 10) values, indicating somewhat drier or more variable climates, respectively. Nevertheless, these values are more negative than Holocene values, demonstrating the climate was significantly wetter. As stated above, Oldowan and Acheulean sites are distributed across western and Southern Arabia (Groucutt and Petraglia, 2012), most likely representing Lower Palaeolithic occupation. In particular, flint scatters from the Nafud – found in conjunction with grassland fauna – indicates hominin occupation of Arabia during MIS 13 or 9 (Rosenberg et al., 2013; Roberts et al., 2018). While these SAHPs could have facilitated hominin occupation of Arabia, it is difficult to relate these to demographic changes in Eurasia due to the persistent presence of Acheulean typologies since ~1.4 Ma (Moncel et al., 2015; Gallotti, 2016). Nonetheless, future studies of Middle Pleistocene population dynamics in Eurasia may benefit from consideration of SAHP timings.

4.3.2. Early *H. sapiens* dispersal

H. sapiens emerged as a distinct species in Africa during the Middle Pleistocene (Hublin et al., 2017; Richter et al., 2017; Scerri et al., 2018b). Behavioural and anatomical modernity evolved gradually throughout the later Middle Pleistocene and into the Upper Pleistocene (McBrearty and Brooks, 2000). Whilst *H. sapiens* dispersals during the Upper Pleistocene led to colonisation of Eurasia, it has been suggested that *H. sapiens* may also have dispersed within the Middle Pleistocene (Breeze et al., 2016). This may be validated by a *H. sapiens* maxilla from Misliya Cave, Israel, dated between 194 and 177 ka (Hershkovitz et al., 2018; but see Sharp and Paces, 2018). Hershkovitz et al. (2018) suggested a dispersal may have occurred during MIS 6e (~191–170 ka).

Similarly, the recent identification of *H. sapiens* at Apidima, Greece, ~210 ka (MIS 7) provides further support for earlier dispersals (Harvati et al., 2019; but see Wade, 2019).

Travertine deposition in the Negev (Waldmann et al., 2010), increase rainfall in the Levant and Dead Sea catchment (Frumkin et al., 1999; Bar-Matthews et al., 2003; Gasse et al., 2015; Torfstein et al., 2015), decreased RC09-166 $\delta D_{\text{leafwax}}$ (Tierney et al., 2017), and increased Saharan run-off (Williams et al., 2015) indicate ameliorated conditions which may have facilitated *H. sapiens* dispersal within MIS 6e (~191–170 ka) (Breeze et al., 2016; Garcea, 2016). Lack of speleothem growth at Mukalla and Hoti Cave and absence of lake formations (Rosenberg et al., 2011, 2012, 2013) indicate the tropical rain belt did not migrate past 14°N during MIS 6. Moreover, absence of speleothem growth in the central Negev (Vaks et al., 2010) also demonstrates that winter Mediterranean precipitation regimes were not substantially enhanced during MIS 6e. Without these widespread changes in regional precipitation, it is unlikely that green landscapes and inter-regional range expansion could have been sustained.

We therefore suggest dispersals may have occurred during SAHP 5 and 6 (MIS 7a and 7e). Y99 $\delta^{18}\text{O}_{\text{ca}}$ reveals SAHP 5 (MIS 7a) was as wet as SAHP 4 (MIS 5e: discussed below), and $\delta^{13}\text{C}_{\text{ca}}$ values demonstrate C₄ grasslands flourished within both SAHP 5 and 6 (Fig. 7). SAHP 5 (~205–195 ka) corresponds to lake formations in northern Arabia (Rosenberg et al., 2013), and the Sahara (Armitage et al., 2007, 2015), central ages of palaeosol formation on the Sinai Peninsula (Roskin et al., 2013) and speleothem growth in the central Negev (Vaks et al., 2010). Thus, not only did pluvial landscapes connect northern Arabia and the Levant (Breeze et al., 2016), but corridors connected northern and Southern Arabia. While archaeological evidence for such an early dispersal is currently very limited, recent dating of the Saffaqah archaeological site demonstrates hominins occupied Arabia during MIS 7, with technological similarities to the Acheulean of Mieso (Ethiopia) (Scerri et al., 2018a). Further evidence is required, however, taken with recent findings from Arabia (Scerri et al., 2018a), the Levant (Hershkovitz et al., 2018) and south-eastern Europe (Harvati et al., 2019), our data suggests MIS 7a enhancement of the monsoon domain could have facilitated *H. sapiens* range expansion into Eurasia.

Furthermore, our data shows that Southern Arabia could have facilitated occupation by *H. sapiens* shortly after their African emergence during MIS 9 (Hublin et al., 2017; Richter et al., 2017). Considering recent discussions of the pan-African origin of *H. sapiens* (Scerri et al., 2018b), we suggest that Arabia may have been frequently occupied by various early *H. sapiens* lineages. The role of Green Arabia as a habitat for early *H. sapiens* may therefore add to ongoing discussions concerning localized adaptations and genetic flow between subdivided populations (Scerri et al., 2018b). The identification of favourable conditions in MIS 7 and 9 will remain of interest if early *H. sapiens* are not identified: i.e. what prevented their expansion into the region at these times?

4.3.3. Late Pleistocene *H. sapiens* dispersal

The dispersal of *H. sapiens* during the Late Pleistocene is a topic of intense debate, with models changing frequently with new fossil finds. Generally, there is an acceptance that formation of green landscapes in the Saharo-Arabian desert belt facilitated dispersals during MIS 5e (~128–121 ka), MIS 5c (~104–93 ka) and MIS 5a (85–71 ka) (Bae et al., 2017; Groucutt et al., 2018; Rabett, 2018), which is supported by the Mukalla and Hoti Cave records. During the last 130 ka, SAHP 4 (127.8 ± 0.626 to 120.3 ± 0.399 ka) was the most intense pluvial period (Fig. 5), which is in good agreement with lake records in Arabia (Rosenberg et al., 2011, 2012, 2013; Matter et al., 2015). Furthermore, $\delta^{13}\text{C}_{\text{ca}}$ values demonstrate a

grassland environment flourished in the now desert areas of Yemen (Fig. 6), which is corroborated by phytolith evidence from Jabal Faya, UAE (Bretzke et al., 2013). SAHP 3 (MIS 5c) and SAHP 2 (MIS 5a) are consistent with intervals of lake formations in Arabia (Petruglia et al., 2012; Rosenberg et al., 2011, 2012, 2013; Parton et al., 2018) during MIS 5c and 5a and it is clear that *H. sapiens* occupied the now desert interior of Arabia within MIS 5a (e.g., Groucutt et al., 2018).

A subsequent dispersal is argued to have taken place during MIS 4–3 (Mellars, 2006; Mellars et al., 2013; Shea, 2008; Rohling et al., 2013; Langgut et al., 2018). A growing body of archaeological evidence shows *H. sapiens* were present in Arabia during MIS 3 (Armitage et al., 2011; Delagnes et al., 2012; Jennings et al., 2016). Whether climatic changes could have facilitated widespread dispersals is a subject of controversial debate (Mellars, 2006; Groucutt et al., 2015a; Bae et al., 2017) as the evidence for increased rainfall during MIS 4–3 is variable between records. It has been argued that punctuated humid intervals in northern Africa and the Levant may have facilitated dispersal during MIS 4–3 (Hoffmann et al., 2016; Timmermann and Friedrich, 2016; Langgut et al., 2018). However, the lack of speleothem growth in Southern Arabia during MIS 4–3 suggest that the monsoons were considerably weaker, did not penetrate into the Arabian Peninsula nor create widespread "green" landscapes. Our assumption is supported by more positive $\delta D_{leafwax}$ values in core RC09-166 from the Gulf of Aden (Fig. 4), indicating lower monsoonal rainfall compared to MIS 5a or the early to middle Holocene in the Horn of Africa and Afar regions. Additional supporting evidence comes from median grain sizes in cores KL 11 (Red Sea) and KL 15 (Gulf of Aden) which are also larger and indicative of more arid climatic conditions during MIS 4–3 (Fig. 4). In contrast, palaeolake formation in the Nafud (northern Saudi Arabia) (Parton et al., 2018) and fluvial activity at Al-Quwayiyah, central Saudi Arabia (McLaren et al., 2009), Yemen (Delagnes et al., 2012), and in Oman (Blechschmidt et al., 2009; Parton et al., 2013, 2015; Hoffmann et al., 2015) have been dated to early MIS 3. Records in Southern Arabia are not corroborated by speleothem growth at Mukalla Cave or Hoti Cave, indicating that the tropical rain-belt was suppressed. This discrepancy may stem from the potential for fluvio-lacustrine and alluvial records to record high intensity, but brief, storm and flooding events (e.g., Rosenberg et al., 2012; Hoffmann et al., 2015); whereas speleothems require prolonged and more substantial changes in regional rainfall. Moreover, brief and intense storms currently occur under modern climates during hot summers, which could mean MIS 3 alluvial records show precipitation regimes were not greatly different than current conditions (Hoffmann et al., 2015). Taken together, MIS 3 precipitation may not have been sustained or intense enough to have substantially impacted environments in Southern Arabia. Despite archaeological evidence for MIS 3 occupation, our findings suggest that MIS 5 interstadials were 'climatic optima' for hominin dispersal; whereas *H. sapiens* dispersal opportunities during MIS 3 may have been more limited or required different behavioural adaptations. If, however, MIS 3 environments could not sustain dispersal (meaning MIS 3 populations can be related to groups that entered during MIS 5), this implies *H. sapiens* persistence throughout MIS 4, a time with very limited evidence for ameliorated conditions (Parton et al., 2015).

5. Conclusion

New ^{230}Th and U-Pb dates for stalagmite Y99 from Mukalla Cave in Yemen allow us to extend the speleothem-based record of continental wetness back to 1.1 Ma BP. In combination with previously published stalagmite records from Southern Arabia (Burns et al., 2001; Fleitmann et al., 2011), at least twenty-one humid intervals with precipitation above $\sim 300 \text{ mm yr}^{-1}$ developed in Southern

Arabia, all occurring during peak interglacial periods or warm substages. Of all SAHPs the early to mid-Holocene humid period was characterised by the least rainfall. Hydrogen and oxygen isotope measurements on water extracted from stalagmite fluid inclusions indicate that enhanced rainfall during SAHPs resulted from an intensification and greater range of the ASM and ISM. This assumption is further supported by the presence of annual laminae in some stalagmites and nearly monthly-resolved oxygen and carbon isotope measurements which indicate a strong seasonal climate during SAHP, with one rainy (monsoon) season during SAHPs. While there is restricted archaeological evidence for hominin occupation beyond 350 ka BP, these landscapes could have facilitated occupation of late *H. erectus* populations. Subsequent SAHPs may have also facilitated the dispersals of early *H. sapiens* soon after their emergence $\sim 300 \text{ ka BP}$.

CRediT authorship contribution statement

Samuel L. Nicholson: Conceptualization, Investigation, Formal analysis, Writing - original draft, Funding acquisition. **Alistair W.G. Pike:** Supervision, Writing - review & editing, Funding acquisition. **Rob Hosfield:** Supervision, Writing - review & editing, Funding acquisition. **Nick Roberts:** Investigation, Formal analysis, Writing - review & editing. **Diana Sahy:** Investigation, Formal analysis, Writing - review & editing. **Jon Woodhead:** Investigation, Formal analysis, Methodology, Writing - review & editing, Funding acquisition. **R. Lawrence Edwards:** Methodology, Writing - review & editing, Funding acquisition. **Stéphane Affolter:** Investigation, Methodology, Formal analysis, Writing - review & editing. **Markus Leuenberger:** Conceptualization, Methodology, Writing - review & editing, Resources. **Stephen J. Burns:** Conceptualization, Resources, Writing - review & editing, Funding acquisition. **Albert Matter:** Conceptualization, Resources, Writing - review & editing, Funding acquisition. **Dominik Fleitmann:** Conceptualization, Methodology, Resources, Supervision, Writing - review & editing, Funding acquisition, Project administration.

Acknowledgements

This work was supported by the AHRC South, West and Wales Doctoral Training Partnership (Grant AH/L503939/1) the Swiss National Science Foundation (Grant PP002-110554/1 to DF and Grant CRSI22-132646/1 to DF and ML), U.S. National Science Foundation (Grant 1702816 to RLE and HC) and the National Natural Science Foundation of China (Grant NSFC 41888101). DF acknowledges support from NERC Isotope Geosciences Facilities Steering Committee (Grant IP-1376-051). We would like to thank the editor and three anonymous reviewers for their constructive comments and suggestions.

Appendix A. Supplementary data

Supplementary data to this article can be found online at <https://doi.org/10.1016/j.quascirev.2019.106112>.

References

- Affolter, S., Fleitmann, D., Leuenberger, M., 2014. New online method for water isotope analysis of speleothem fluid inclusions using laser absorption spectroscopy (WS-CRDS). *Clim. Past* 10, 1291–1304.
- Affolter, S., Häuselmann, A.D., Fleitmann, D., Häuselmann, P., Leuenberger, M., 2015. Triple isotope (δD , $\delta^{17}\text{O}$, $\delta^{18}\text{O}$) study on precipitation, drip water and speleothem fluid inclusions for a Western Central European cave (NW Switzerland). *Quat. Sci. Rev.* 127, 73–89.
- Al-ameri, A., Schneider, M., Abu Lohom, N., Sprenger, C., 2014. The hydrogen (δD) and oxygen ($\delta^{18}\text{O}$) isotopic composition of Yemen's rainwater. *Arabian J. Sci.*

- Eng. 39, 423–436.
- Almogi-Labbin, A., Schmiedl, G., Hemleben, C., Siman-Tov, R., Segl, M., Meischner, D., 2000. The influence of the NE winter monsoon on productivity changes in the Gulf of Aden, NW Arabian Sea, during the last 530 ka as recorded by foraminifera. *Mar. Micropaleontol.* 40, 295–319.
- Armitage, S.J., Bristow, C.S., Drake, N.A., 2015. West African monsoon dynamics inferred from abrupt fluctuations of Lake Mega-Chad. *Proc. Natl. Acad. Sci.* 112, 8543–8548.
- Armitage, S.J., Drake, N.A., Stokes, S., El-Hawat, A., Salem, M.J., White, K., Turner, P., McLaren, S.J., 2007. Multiple phases of north African humidity recorded in lacustrine sediments from the Fazzan basin, Libyan Sahara. *Quat. Geochronol.* 2, 181–186.
- Armitage, S.J., Jasim, S.A., Marks, A.E., Parker, A.G., Usik, V.I., Uerpmann, H.-P., 2011. The Southern Route “Out of Africa”: Evidence for an Early Expansion of Modern Humans into Arabia. *Science* 331 (6016), 453–456.
- Bae, C.J., Douka, K., Petraglia, M.D., 2017. On the origin of modern humans: Asian perspectives. *Science* 358 (6368), eaai9067.
- Bailey, G.N., Devès, M.H., Inglis, R.H., Meredith-Williams, M.G., Momber, G., Sakellariou, D., Sinclair, A.G.M., Rousakis, G., Al Ghamdi, S., Alsharekh, A.M., 2015. Blue Arabia: Palaeolithic and underwater survey in SW Saudi Arabia and the role of coasts in Pleistocene dispersals. *Quat. Int.* 382, 42–57.
- Bajo, P., Hellstrom, J., Frisia, S., Drysdale, R., Black, J., Woodhead, J., Borsato, A., Zanchetta, G., Wallace, M.W., Regattieri, E., Haese, R., 2016. Cryptic diagenesis and its implications for speleothem geochronologies, 148, 17–28.
- Baker, A., Ito, E., Smart, P.L., McEwan, R.F., 1997. Elevated and variable values of ^{13}C in speleothems in a British cave system. *Chem. Geol.* 136, 263–270.
- Bar-Matthews, M., Ayalon, A., Gilmour, M., Matthews, A., Hawkesworth, C.J., 2003. Sea – land oxygen isotopic relationships from planktonic foraminifera and speleothems in the Eastern Mediterranean region and their implication for paleorainfall during interglacial intervals. *Geochem. Cosmochim. Acta* 67, 3181–3199.
- Bar-Matthews, M., Ayalon, A., Matthews, A., Sass, E., Halicz, L., 1996. Carbon and oxygen isotope study of the active water-carbonate system in a karstic Mediterranean cave: implications for paleoclimate research in semiarid regions. *Geochem. Cosmochim. Acta* 60, 337–347.
- Beck, J.W., Zhou, W., Li, C., Wu, Z., White, L., Xian, F., Kong, X., An, Z., 2018. A 550,000-year record of East Asian monsoon rainfall from ^{10}Be in loess. *Science* 360, 877–881. LP.
- Berger, A., Loutre, M.F., 1991. Insolation values for the climate of the last 10 million years. *Quat. Sci. Rev.* 10, 297–317.
- Berger, A., Loutre, M.F., 1999. Parameters of the Earth's orbit for the last 5 Million years in 1 kyr resolution. Supplement to: berger, A.; Loutre, M F (1991): insolation values for the climate of the last 10 million of years. *Quat. Sci. Rev.* 10 (4), 297–317. [https://doi.org/10.1016/0277-3791\(91\)90033-Q](https://doi.org/10.1016/0277-3791(91)90033-Q).
- Blechschmidt, I., Matter, A., Preusser, F., Rieke-Zapp, D., 2009. Monsoon triggered formation of Quaternary alluvial megafans in the interior of Oman. *Geomorphology* 110 (3–4), 128–139.
- Borsato, A., Quinif, Y., Bini, A., Dublyansky, Y., 2003. Open-system alpine speleothems: implications for U-series dating and palaeoclimate reconstructions. *Studi Trentini Sci. Nat. Acta Geol.* 80, 71–83.
- Breeze, P.S., Drake, N.A., Groucutt, H.S., Parton, A., Jennings, R.G.P., White, T.S., Clark-Balzan, L., Shipton, C., Scerri, E.M.L.L., Stimpson, C.M., Crassard, R., Hilbert, Y., Alsharekh, A., Al-Omari, A., Petraglia, M.D., Clarke-Balzan, L., Shipton, C., White, T.S., Scerri, E.M.L.L., Stimpson, C.M., Clark-Balzan, L., Shipton, C., Scerri, E.M.L.L., Stimpson, C.M., Crassard, R., Hilbert, Y., Alsharekh, A., Al-Omari, A., Petraglia, M.D., 2015. Remote sensing and GIS techniques for reconstructing Arabian palaeohydrology and identifying archaeological sites. *Quat. Int.* 382, 98–119.
- Breeze, P.S., Groucutt, H.S., Drake, N.A., White, T.S., Jennings, R.P., Petraglia, M.D., 2016. Palaeohydrological corridors for hominin dispersals in the Middle East ~250–70,000 years ago. *Quat. Sci. Rev.* 144, 155–185.
- Bretzke, K., Armitage, S.J., Parker, A.G., Walkington, H., Uerpmann, H.P., 2013. The environmental context of Paleolithic settlement at Jebel Faya, Emirate Sharjah, UAE. *Quat. Int.* 300, 83–93.
- Bretzke, K., Yousif, E., Jasim, S., 2016. Filling in the gap – the Acheulean site Suhailah 1 from the central region of the Emirate of Sharjah, UAE. *Quat. Int.* 466 (Part A), 23–32.
- Burns, S.J., Fleitmann, D., Matter, A., Neff, U., Mangini, A., 2001. Speleothem evidence from Oman for continental pluvial events during interglacial periods. *Geology* 29, 623–626.
- Burns, S.J., Matter, A., Frank, N., Mangini, A., 1998. Speleothem-based paleoclimate record from northern Oman. *Geology* 26, 499–502.
- Cerling, T.E., Wynn, J.G., Andanje, S.A., Bird, M.I., Korir, D.K., Levin, N.E., MacE, W., MacHaria, A.N., Quade, J., Remien, C.H., 2011. Woody cover and hominin environments in the past 6-million years. *Nature* 476, 51–56.
- Chauhan, P.R., 2009. Early Homo occupation near the gate of tears: examining the Paleoanthropological records of Djibouti and Yemen. In: *Vertebrate Paleobiology and Paleoanthropology*.
- Cheng, H., Edwards, R.L., Sinha, A., Spötl, C., Yi, L., Chen, S., Kelly, M., Kathayat, G., Wang, X., Li, X., Kong, X., Wang, Y., Ning, Y., Zhang, H., 2016. The Asian monsoon over the past 640,000 years and ice age terminations. *Nature* 534, 640–646.
- Cheng, H., Fleitmann, D., Edwards, R.L., Wang, X., Cruz, F.W., Auler, A.S., Mangini, A., Wang, Y., Kong, X., Burns, S.J., Matter, A., 2009. Timing and structure of the 8.2 kyr B.P. event inferred from δ 18O records of stalagmites from China, Oman, and Brazil. *Geology* 37, 1007–1010.
- Cheng, H., Lawrence Edwards, R., Shen, C.C., Polyak, V.J., Asmerom, Y., Woodhead, J., Hellstrom, J., Wang, Y., Kong, X., Spötl, C., Wang, X., Calvin Alexander, E., 2013. Improvements in ^{230}Th dating, ^{230}Th and ^{234}U half-life values, and U-Th isotopic measurements by multi-collector inductively coupled plasma mass spectrometry. *Earth Planet. Sci. Lett.* 371–372, 82–91.
- Clark, I., Fritz, P., 1997. Environmental Isotopes in Hydrogeology. Lewis Publishers, New York.
- Clemens, S.C., Prell, W.L., 2003. A 350,000 year summer-monsoon multi-proxy stack from the Owen ridge, northern Arabian Sea. In: *Marine Geology*, pp. 35–51.
- Coogan, L.A., Parrish, R.R., Roberts, N.M.W., 2016. Early hydrothermal carbon uptake by the upper oceanic crust: insight from in situ U-Pb dating. *Geology* 44 (2), 147–150.
- Crémère, A., Lepland, A., Chand, S., Sahy, D., Condon, D.J., Noble, S.R., Martma, T., Thorsnes, T., Sauer, S., Brunstad, H., 2016. Timescales of methane seepage on the Norwegian margin following collapse of the Scandinavian Ice Sheet. *Nat. Commun.* 7, 11509.
- Dansgaard, W., 1964. Stable isotopes in precipitation. *Tellus* 16, 436–468.
- Delagnes, A., Tribolo, C., Bertran, P., Brenet, M., Crassard, R., Jaubert, J., Khalidi, L., Mercier, N., Nomade, S., Peigné, S., Sitzia, L., Tournebiche, J.-F., Al-Halibi, M., Al-Mosabi, A., Macchiarelli, R., 2012. Inland human settlement in southern Arabia 55,000 years ago. New evidence from the Wadi Surdud Middle Palaeolithic site complex, western Yemen. *J. Hum. Evol.* 63, 452–474.
- deMenocal, P.B., 1995. Plio-pleistocene African climate. *Science* 270, 53–59.
- Dennis, P.F., Rowe, P.J., Atkinson, T.C., 2001. The recovery and isotopic measurement of water from fluid inclusions in speleothems. *Geochem. Cosmochim. Acta* 65, 871–884.
- Drake, N., Breeze, P., 2016. Climate change and modern human occupation of the Sahara from MIS 6–2. In: *Africa from MIS*, vols. 6–2, pp. 103–122.
- Drake, N.A., Blench, R.M., Armitage, S.J., Bristow, C.S., White, K.H., 2011. Ancient watercourses and biogeography of the Sahara explain the peopling of the desert. *Proc. Natl. Acad. Sci.* 108, 458–462.
- El-Shenawy, M.I., Kim, S.-T., Schwarcz, H.P., Asmerom, Y., Polyak, V.J., 2018. Speleothem evidence for the greening of the Sahara and its implications for the early human dispersals out of sub-Saharan Africa. *Quat. Sci. Rev.* 188, 67–76.
- Engel, M., Matter, A., Parker, A.G., Parton, A., Petraglia, M.D., Preston, G.W., Preusser, F., 2017. Lakes or wetlands? A comment on ‘The middle Holocene climatic records from Arabia: reassessing lacustrine environments, shift of ITCZ in Arabian Sea, and impacts of the southwest Indian and African monsoons’ by Enzel et al. *Glob. Planet. Chang.* 148, 258–267.
- Enzel, Y., Kushnir, Y., Quade, J., 2015. The middle Holocene climatic records from Arabia: reassessing lacustrine environments, shift of ITCZ in Arabian Sea, and impacts of the southwest Indian and African monsoons. *Glob. Planet. Chang.* 129, 69–91.
- Fernandes, C.A., Rohling, E.J., Siddall, M., 2006. Absence of post-Miocene Red Sea land bridges: biogeographic implications. *J. Biogeogr.* 33 (6), 961–966.
- Fleitmann, D., 1997. Klastischer Eintrag in das Rote Meer und den Golf von Aden durch den Arabischen Monsun-Untersuchungen an Kolbenlot-Kernen. Masters thesis. Diplom-Arbeit, Institut und Museum für Geologie und Paläontologie der Georg-August-Universität zu Göttingen.
- Fleitmann, D., Burns, S.J., Mangini, A., Mudelsee, M., Kramers, J., Villa, I., Neff, U., Al-Subbary, A.A., Buetner, A., Hipppler, D., Matter, A., 2007. Holocene ITCZ and Indian monsoon dynamics recorded in stalagmites from Oman and Yemen (Socotra). *Quat. Sci. Rev.* 26, 170–188.
- Fleitmann, D., Burns, S.J., Mudelsee, M., Neff, U., Kramers, J., Mangini, A., Matter, A., 2003a. Holocene forcing of the Indian monsoon recorded in a stalagmite from Southern Oman. *Science* 300, 1737–1739.
- Fleitmann, D., Burns, S.J., Neff, U., Mangini, A., Matter, A., 2003b. Changing moisture sources over the last 330,000 years in Northern Oman from fluid-inclusion evidence in speleothems. *Quat. Res.* 60, 223–232.
- Fleitmann, D., Burns, S.J., Neff, U., Mudelsee, M., Mangini, A., Matter, A., 2004. Palaeoclimatic interpretation of high-resolution oxygen isotope profiles derived from annually laminated speleothems from Southern Oman. In: *Quaternary Science Reviews*, pp. 935–945.
- Fleitmann, D., Burns, S.J., Pekala, M., Mangini, A., Al-Subbary, A., Al-Awah, M., Kramers, J., Matter, A., 2011. Holocene and Pleistocene pluvial periods in Yemen, southern Arabia. *Quat. Sci. Rev.* 30, 783–787.
- Fleitmann, D., Matter, A., 2009. The speleothem record of climate variability in Southern Arabia. *Compt. Rendus Geosci.* 341, 633–642.
- Fick, S.E., Hijmans, R.J., 2017. Worldclim 2: new 1-km spatial resolution climate surfaces for global land areas. *Int. J. Climatol.* 37, 4302–4315.
- Frumkin, A., Ford, D.C., Schwarze, H.P., 1999. Continental oxygen isotopic record of the last 170,000 years in Jerusalem. *Quat. Res.* 51, 317–327.
- Gallotti, R., 2016. The East African origin of the western European Acheulean technology: fact or paradigm? *Quat. Int.* 411, 9–24.
- Garcea, E.A.A., 2016. Dispersals out of Africa and back to Africa: modern origins in north Africa. *Quat. Int.* 408, 79–89.
- Gasse, F., Vidal, L., Van Campo, E., Demory, F., Develle, A.L., Tachikawa, K., Elias, A., Bard, E., Garcia, M., Sonzogni, C., Thouveny, N., 2015. Hydroclimatic changes in northern Levant over the past 400,000 years. *Quat. Sci. Rev.* 111, 1–8.
- Gat, J.R., Carmi, I., 1970. Evolution of the isotopic composition of atmospheric waters in the Mediterranean Sea area. *J. Geophys. Res.* 75, 3039–3048.
- Gierz, P., Werner, M., Lohmann, G., 2017. Simulating climate and stable water isotopes during the Last Interglacial using a coupled climate-isotope model. *J. Adv. Model. Earth Syst.* 9, 2027–2045.
- Grant, K.M., Grimm, R., Mikolajewicz, U., Marino, G., Ziegler, M., Rohling, E.J., 2016.

- The timing of Mediterranean sapropel deposition relative to insolation, sea-level and African monsoon changes. *Quat. Sci. Rev.* 140, 125–141.
- Grant, K.M., Rohling, E.J., Bar-Matthews, M., Ayalon, A., Medina-Elizalde, M., Ramsey, C.B., Satow, C., Roberts, A.P., 2012. Rapid coupling between ice volume and polar temperature over the past 50,000 years. *Nature* 491, 744–747.
- Grant, K.M., Rohling, E.J., Westerhold, T., Zabel, M., Heslop, D., Konijnendijk, T., Lourens, L., 2017. A 3 million year index for North African humidity/aridity and the implication of potential pan-African Humid periods. *Quat. Sci. Rev.* 171, 100–118.
- Groucutt, H.S., Grün, R., Zalmout, I.A.S., Drake, N.A., Armitage, S.J., Candy, I., Clark-Wilson, R., Louys, J., Breeze, P.S., Duval, M., Buck, L.T., Kivell, T.L., Pomeroy, E., Stephens, N.B., Stock, J.T., Stewart, M., Price, G.J., Kinsley, L., Sung, W.W., Alsharekh, A., Al-Omari, A., Zahir, M., Memesh, A.M., Abdulshakoor, A.J., Al-Masari, A.M., Bahameem, A.A., Al Murayyi, K.M.S., Zahrani, B., Scerri, E.L.M., Petraglia, M.D., Gramp, R., Zalmout, I.A., Drake, N.A., Armitage, S.J., Candy, I., Clark-Wilson, R., Louys, J., Breeze, P.S., Duval, M., Buck, L.T., Kivell, T.L., Pomeroy, E., Stephens, N.B., Stock, J.T., Stewart, M., Price, G.J., Kinsley, L., Wai Sung, W., Alsharekh, A., Al-Omari, A., Zahir, M., Memesh, A.M., Abdulshakoor, A.J., Al-Masari, A.M., Bahameem, A.A., S Al Murayyi, K.M., Zahrani, B., M Scerri, E.L., Petraglia, M.D., 2018. Homo sapiens in Arabia by 85,000 years ago. *Nat. Ecol. Evol.* 2, 800–809.
- Groucutt, H.S., Petraglia, M.D., 2012. The prehistory of the Arabian peninsula: deserts, dispersals, and demography. *Evol. Anthropol.* 21, 113–125.
- Groucutt, H.S., Petraglia, M.D., Bailey, G., Scerri, E.M.L.L., Parton, A., Clark-Balzan, L., Jennings, R.P., Lewis, L., Blinkhorn, J., Drake, N.A., Breeze, P.S., Inglis, R.H., Devès, M.H., Meredith-Williams, M., Boivin, N., Thomas, M.G., Scally, A., Devès, M.H., Meredith-Williams, M., Boivin, N., Thomas, M.G., Scally, A., 2015a. Rethinking the dispersal of *Homo sapiens* out of Africa. *Evol. Anthropol.* 24, 149–164.
- Groucutt, H.S., Shipton, C., Alsharekh, A., Jennings, R., Scerri, E.M.L., Petraglia, M.D., 2015b. Late Pleistocene lakeshore settlement in northern Arabia: middle Palaeolithic technology from Jebel Katefah, Jubbah. *Quat. Int.* 382, 215–236.
- Harvati, K., Röding, C., Bosman, A.M., Karakostis, F.A., Grün, R., Stringer, C., Karkanas, P., Thompson, N.C., Koutoulidis, V., Moulopoulos, L.A., Gorgoulis, V.G., Koulikoussa, M., 2019. Apidima Cave fossils provide earliest evidence of *Homo sapiens* in Eurasia. *Nature* 571, 500–504.
- Herold, M., Lohmann, G., 2009. Eemian tropical and subtropical African moisture transport: an isotope modelling study. *Clim. Dyn.* 33, 1075–1088.
- Hershkovitz, I., Weber, G.W., Quam, R., Duval, M., Grün, R., Kinsley, L., Ayalon, A., Bar-Matthews, M., Valladas, H., Mercier, N., Arsuaga, J.L., Martín-Torres, M., Bermúdez de Castro, J.M., Fornai, C., Martín-Francés, L., Sarig, R., May, H., Krenn, V.A., Slon, V., Rodríguez, L., García, R., Lorenzo, C., Carretero, J.M., Frumkin, A., Shahack-Gross, R., Bar-Yosef Mayer, D.E., Cui, Y., Wu, X., Peled, N., Groman-Yaroslavski, I., Weissbrod, L., Yeshurun, R., Tsatskin, A., Zaidner, Y., Weinstein-Evron, M., 2018. The earliest modern humans outside Africa. *Science* 359, 456–459. LP.
- Hill, C.A., Poljak, V.J., Asmerom, Y., Provencio, P., 2016. Constraints on a Late Cretaceous uplift, denudation, and incision of the Grand Canyon region, southwestern Colorado Plateau, USA, from U-Pb dating of lacustrine limestone. *Tectonics* 35, 896–906.
- Hoffmann, D.L., Rogerson, M., Spötl, C., Luetscher, M., Vance, D., Osborne, A.H., Fello, N.M., Moseley, G.E., 2016. Timing and causes of North African wet phases during the last glacial period and implications for modern human migration. *Sci. Rep.* 6.
- Hoffmann, G., Rupprechter, M., Rahn, M., Preusser, F., 2015. Fluvio-Lacustrine deposits reveal precipitation pattern in SE Arabia during early MIS 3. *Quat. Int.* 382, 145–153.
- Hublin, J.J., Ben-Ncer, A., Bailey, S.E., Freidline, S.E., Neubauer, S., Skinner, M.M., Bergmann, I., Le Cabec, A., Benazzi, S., Harvati, K., Gunz, P., 2017. New fossils from Jebel Irhoud, Morocco and the pan-African origin of *Homo sapiens*. *Nature* 546, 289–292.
- Jennings, R.P., Parton, A., Clark-Balzan, L., White, T.S., Groucutt, H.S., Breeze, P.S., Parker, A.G., Drake, N.A., Petraglia, M.D., 2016. Human occupation of the northern Arabian interior during early Marine Isotope Stage 3. *J. Quat. Sci.* 31 (8), 953–966.
- Jennings, R.P., Shipton, C., Breeze, P., Cuthbertson, P., Bernal, M.A., Wedge, W.M.C.O., Drake, N.A., White, T.S., Groucutt, H.S., Parton, A., Clark-Balzan, L., Stimpson, C., al Omari, A.A., Alsharekh, A., Petraglia, M.D., 2015a. Multi-scale Acheulean landscape survey in the Arabian Desert. *Quat. Int.* 382, 58–81.
- Jennings, R.P., Singarayer, J., Stone, E.J., Krebs-Kanzow, U., Khon, V., Nisancioğlu, K.H., Pfeiffer, M., Zhang, X., Parker, A., Parton, A., Groucutt, H.S., White, T.S., Drake, N.A., Petraglia, M.D., 2015b. The greening of Arabia: multiple opportunities for human occupation of the Arabian Peninsula during the Late Pleistocene inferred from an ensemble of climate model simulations. *Quat. Int.* 382, 181–199.
- Kahlke, R.D., García, N., Kostopoulos, D.S., Lacombat, F., Lister, A.M., Mazza, P.P.A., Spassov, N., Titov, V.V., 2011. Western Palaearctic palaeoenvironmental conditions during the Early and early Middle Pleistocene inferred from large mammal communities, and implications for hominin dispersals in Europe. *Quat. Sci. Rev.* 30 (11–12), 1368–1395.
- Kutzbach, J.E., Chen, G., Cheng, H., Edwards, R.L., Liu, Z., 2014. Potential role of winter rainfall in explaining increased moisture in the Mediterranean and Middle East during periods of maximum orbitally-forced insolation seasonality. *Clim. Dyn.* 42, 1079–1095.
- Lambeck, K., Purcell, A., Flemming, N.C., Vita-Finzi, C., Alsharekh, A.M., Bailey, G.N., 2011. Sea level and shoreline reconstructions for the Red Sea: isostatic and tectonic considerations and implications for hominin migration out of Africa. *Quat. Sci. Rev.* 30 (25–26), 3542–3574.
- Langgut, D., Almogi-Labin, A., Bar-Matthews, M., Pickarski, N., Weinstein-Evron, M., 2018. Evidence for a humid interval at ~56–44 ka in the Levant and its potential link to modern humans dispersals out of Africa. *J. Hum. Evol.* 124, 75–90.
- Larrasoana, J.C., Roberts, A.P., Rohling, E.J., 2013. Dynamics of green Sahara periods and their role in hominin evolution. *PLoS One* 8.
- Larrasoana, J.C., Roberts, A.P., Rohling, E.J., Winklhofer, M., Wehausen, R., 2003. Three million years of monsoon variability over the northern Sahara. *Clim. Dyn.* 21, 689–698.
- Lisiecki, L.E., Raymo, M.E., 2005. A Pliocene-Pleistocene stack of 57 globally distributed benthic δ 18O records. *Paleoceanography* 20, 1–17.
- Maslin, M.A., Brierley, C.M., Milner, A.M., Shultz, S., Trauth, M.H., Wilson, K.E., 2014. East African climate pulses and early human evolution. *Quat. Sci. Rev.* 101, 1–17.
- Matthews, A., Ayalon, A., Bar-Matthews, M., 2000. D/H ratios of fluid inclusions of Soreq Cave (Israel) speleothems as a guide to the Eastern Mediterranean Meteoric Line relationship in the last 120 kyr. *Chem. Geol.* 166, 183–191.
- Matter, A., Neubert, E., Preusser, F., Rosenberg, T., Al-Wagdani, K., 2015. Palaeoenvironmental implications derived from lake and sabkha deposits of the southern Rub' al-Khal, Saudi Arabia and Oman. *Quat. Int.* 382, 120–131.
- McBrearty, S., Brooks, A.S., 2000. The revolution that wasn't: a new interpretation of the origin of modern human behavior. *J. Hum. Evol.* 39 (5), 453–563.
- McDermott, F., 2004. Palaeo-climate reconstruction from stable isotope variations in speleothems: review. In: *Quaternary Science Reviews*, pp. 901–918.
- McGarry, S., Bar-Matthews, M., Matthews, A., Vaks, A., Schilman, B., Ayalon, A., 2004. Constraints on hydrological and paleotemperature variations in the Eastern Mediterranean region in the last 140 ka given by the δD values of speleothem fluid inclusions. *Quat. Sci. Rev.* 23, 919–934.
- McLaren, S.J., Al-Juaidi, F., Bateman, M.D., Millington, A.C., 2009. First evidence for episodic flooding events in the arid interior of central Saudi Arabia over the last 60 ka. *J. Quat. Sci.* 24, 198–207.
- Meckler, A.N., Affolter, S., Dublyansky, Y.V., Krüger, Y., Vogel, N., Bernasconi, S.M., Frenz, M., Kipfer, R., Leuenberger, M., Spötl, C., Carolin, S., Cobb, K.M., Moerman, J., Adkins, J.F., Fleitmann, D., 2015. Glacial-interglacial temperature change in the tropical West Pacific: a comparison of stalagmite-based paleothermometers. *Quat. Sci. Rev.* 127, 90–116.
- Mellars, P., 2006. Why did modern human populations disperse from Africa ca. 60,000 years ago? A new model. *Proc. Natl. Acad. Sci.* 103, 9381–9386.
- Mellars, P., Gori, K.C., Carr, M., Soares, P.A., Richards, M.B., 2013. Genetic and archaeological perspectives on the initial modern human colonization of southern Asia. *Proc. Natl. Acad. Sci.* 110, 10699–10704.
- Mitchell, T.D., Jones, P.D., 2005. An improved method of constructing a database of monthly climate observations and associated high-resolution grids. *Int. J. Climatol.* 25, 693–712.
- Moncel, M.H., Ashton, N., Lamotte, A., Tuffreau, A., Cliquet, D., Despriée, J., 2015. The early Acheulian of north-western Europe. *J. Anthropol. Archaeol.* 40, 302–331.
- Muttoni, G., Scardia, G., Kent, D.V., 2010. Human migration into Europe during the late Early Pleistocene climate transition. *Palaeogeogr. Palaeoclimatol. Palaeoecol.* 296, 79–93.
- Neff, U., Burns, S.J., Mangini, A., Mudelsee, M., Fleitmann, D., Matter, A., 2001. Strong coherence between solar variability and the monsoon in Oman between 9 and 6 kyr ago. *Nature* 411, 290–293.
- Parton, A., Clark-Balzan, L., Parker, A.G., Preston, G.W., Sung, W.W., Breeze, P.S., Leng, M.J., Groucutt, H.S., White, T.S., Alsharekh, A., Petraglia, M.D., 2018. Middle-late quaternary palaeoclimate variability from lake and wetland deposits in the Nefud Desert, Northern Arabia. *Quat. Sci. Rev.* 202, 78–97.
- Parton, A., Farrant, A.R., Leng, M.J., Schwenninger, J.L., Rose, J.I., Uerpmann, H.P., Parker, A.G., 2013. An early MIS 3 pluvial phase in Southeast Arabia: climatic and archaeological implications. *Quat. Int.* 300, 62–74.
- Parton, A., White, T.S., Parker, A.G., Breeze, P.S., Jennings, R., Groucutt, H.S., Petraglia, M.D., 2015. Orbital-scale climate variability in Arabia as a potential motor for human dispersals. *Quat. Int.* 382, 82–97.
- Pedgley, D.E., 1969. Cyclones along the Arabian coast. *Weather* 24, 456–470.
- Petraglia, M.D., Alsharekh, A., Breeze, P., Clarkson, C., Crassard, R., Drake, N.A., Groucutt, H.S., Jennings, R., Parker, A.G., Parton, A., Roberts, R.G., Shipton, C., Matheson, C., al Omari, A., Veall, M.A., 2012. Hominin dispersals into the Nefud desert and middle Palaeolithic settlement along the Jubbah palaeolake, northern Arabia. *PLoS One* 7.
- Petraglia, M.D., Alsharekh, A.M., Crassard, R., Drake, N.A., Groucutt, H., Parker, A.G., Roberts, R.G., 2011. Middle Paleolithic occupation on a marine isotope stage 5 lakeshore in the Nefud desert, Saudi Arabia. *Quat. Sci. Rev.* 30, 1555–1559.
- Profico, A., di Vincenzo, F., Gagliardi, L., Piperno, M., Manzi, G., 2016. Filling the gap: Human cranial remains from Gombore II (Melka kunture, Ethiopia; ca. 850 ka) and the origin of *Homo heidelbergensis*. *J. Anthropol. Sci.* 94, 41–63.
- Quade, J., Dente, E., Armon, M., Ben Dor, Y., Morin, E., Adam, O., Enzel, Y., 2018. Megalakes in the Sahara? A review. *Quat. Res. (U.S.)* 90, 253–275.
- Rabett, R.J., 2018. The success of failed *Homo sapiens* dispersals out of Africa and into Asia. *Nat. Ecol. Evol.* 2, 212–219.
- Railsback, L.B., Gibbard, P.L., Head, M.J., Voarintsoa, N.R.G., Toucanne, S., 2015. An optimized scheme of lettered marine isotope substages for the last 1.0 million years, and the chronostratigraphic nature of isotope stages and substages. *Quat. Sci. Rev.* 111, 94–106.
- Richter, D., Grün, R., Joannes-Boyau, R., Steele, T.E., Amani, F., Rué, M., Fernandes, P.,

- Raynal, J.P., Geraads, D., Ben-Ncer, A., Hublin, J.J., McPherron, S.P., 2017. The age of the hominin fossils from Jebel irhoud, Morocco, and the origins of the middle stone age. *Nature* 546, 293–296.
- Roberts, N.M.W., Rasbury, E.T., Parrish, R.R., Smith, C.J., Horstwood, M.S.A., Condon, D.J., 2017. A calcite reference material for LA-ICP-MS U-Pb geochronology. *Geochem. Geophys. Geosyst.* 18 (7), 2807–2814.
- Roberts, P., Stewart, M., Alagaili, A.N., Breeze, P., Candy, I., Drake, N., Groucutt, H.S., Scerri, E.M.L., Lee-Thorp, J., Louys, J., Zalmout, I.S., Al-Mufarreh, Y.S.A., Zech, J., Alsharekh, A.M., al Omari, A., Boivin, N., Petraglia, M., 2018. Fossil herbivore stable isotopes reveal middle Pleistocene hominin palaeoenvironment in 'Green' Arabia. *Nat. Ecol. Evol.* 2, 1871–1878.
- Rohling, E.J., Grant, K.M., Roberts, A.P., Larrasoña, J.-C., 2013. Paleoclimate variability in the mediterranean and Red Sea regions during the last 500,000 years. *Curr. Anthropol.* 54, S183–S201.
- Rohling, E.J., Marino, G., Grant, K.M., 2015. Mediterranean climate and oceanography, and the periodic development of anoxic events (sapropels). *Earth Sci. Rev.* 143, 62–97.
- Rose, J.I., Usik, V.I., Marks, A.E., Hilbert, Y.H., Galletti, C.S., Parton, A., Geiling, J.M., Černý, V., Morley, M.W., Roberts, R.G., 2011. The Nubian complex of Dhofar, Oman: an african middle stone age industry in southern Arabia. *PLoS One* 6.
- Rosenberg, T.M., Preusser, F., Blechschmidt, I., Fleitmann, D., Jagher, R., Matter, A., 2012. Late Pleistocene palaeolake in the interior of Oman: a potential key area for the dispersal of anatomically modern humans out-of-Africa? *J. Quat. Sci.* 27, 13–16.
- Rosenberg, T.M., Preusser, F., Fleitmann, D., Schwalb, A., Penkman, K., Schmid, T.W., Al-Shanti, M.A., Kadi, K., Matter, A., 2011. Humid periods in southern Arabia: windows of opportunity for modern human dispersal. *Geology* 39, 1115–1118.
- Rosenberg, T.M., Preusser, F., Risberg, J., Plíkk, A., Kadi, K.A., Matter, A., Fleitmann, D., 2013. Middle and Late Pleistocene humid periods recorded in palaeolake deposits of the Nafud desert, Saudi Arabia. *Quat. Sci. Rev.* 70, 109–123.
- Roskin, J., Katra, I., Porat, N., Zilberman, E., 2013. Evolution of middle to late Pleistocene sandy calcareous paleosols underlying the northwestern Negev desert Dunefield (Israel). *Palaeogeogr. Palaeoclimatol. Palaeoecol.* 387, 134–152.
- Rowe, P.J., Mason, J.E., Andrews, J.E., Marca, A.D., Thomas, L., Van Calsteren, P., Jex, C.N., Vonhof, H.B., Al-Omari, S., 2012. Speleothem isotopic evidence of winter rainfall variability in northeast Turkey between 77 and 6 ka. *Quat. Sci. Rev.* 45, 60–72.
- Scerri, E.M.L., Shipton, C., Clark-Balzan, L., Frouin, M., Schwenninger, J.-L., Groucutt, H.S., Breeze, P.S., Parton, A., Blinkhorn, J., Drake, N.A., Jennings, R., Cuthbertson, P., Omari, A., Al, Alsharekh, A.M., Petraglia, M.D., 2018a. The expansion of later Acheulean hominins into the Arabian Peninsula. *Sci. Rep.* 8, 17165.
- Scerri, E.M.L., Thomas, M.G., Manica, A., Gunz, P., Stock, J.T., Stringer, C., Grove, M., Groucutt, H.S., Timmermann, A., Rightmire, G.P., D'Errico, F., Tryon, C.A., Drake, N.A., Brooks, A.S., Dennell, R.W., Durbin, R., Henn, B.M., Lee-Thorp, J., DeMenocal, P., Petraglia, M.D., Thompson, J.C., Scally, A., Chikhi, L., 2018b. Did our species evolve in subdivided populations across Africa, and why does it matter? *Trends Ecol. Evol.* 33, 582–594.
- Sharp, W.D., Paces, J.B., 2018. Comment on "The earliest modern humans outside Africa". *Science* 362, eaat6598.
- Shea, J.J., 2008. Transitions or turnovers? Climatically-forced extinctions of Homo sapiens and Neanderthals in the East mediterranean levant. *Quat. Sci. Rev.* 27, 2253–2270.
- Scholz, D., Tolzmann, J., Hoffmann, D.L., Jochum, K.P., Spötl, C., Riechelmann, D.F.C., 2014. Diagenesis of speleothems and its effects on the accuracy of 230Th/U ages. *Chem. Geol.* 387, 74–86.
- Shultz, S., Maslin, M., 2013. Early human speciation, brain expansion and dispersal influenced by african climate pulses. *PLoS One* 8.
- Stimpson, C.M., Lister, A., Parton, A., Clark-Balzan, L., Breeze, P.S., Drake, N.A., Groucutt, H.S., Jennings, R., Scerri, E.M.L., White, T.S., Zahir, M., Duval, M., Grün, R., Al-Omari, A., Al Murayyi, K.S.M., Zalmout, I.S., Mufarreh, Y.A., Memesh, A.M., Petraglia, M.D., 2016. Middle Pleistocene vertebrate fossils from the Nefud desert, Saudi Arabia: implications for biogeography and palaeoecology. *Quat. Sci. Rev.* 143, 13–36.
- Thomas, H., Geraads, D., Janjou, D., Vaslet, D., Memesh, A., Billiou, D., Bocherens, H., Dobigny, G., Eisenmann, V., Gayet, M., Lapparent de Broin, F., Petter, G., Halawani, M., 1998. First Pleistocene faunas from the Arabian peninsula: an Nafud desert, Saudi Arabia. *Comptes Rendus Acad. Sci. - Ser. IIa Earth Planet. Sci.* 326, 145–152.
- Tierney, J.E., deMenocal, P.B., Zander, P.D., 2017. A climatic context for the out-of-Africa migration. *Geology* 45, 1023–1026.
- Timmermann, A., Friedrich, T., 2016. Late Pleistocene climate drivers of early human migration. *Nature* 538, 92–95.
- Torfstein, A., Goldstein, S.L., Kushnir, Y., Enzel, Y., Haug, G., Stein, M., 2015. Dead Sea drawdown and monsoonal impacts in the Levant during the last interglacial. *Earth Planet. Sci. Lett.* 412, 235–244.
- Tzedakis, P.C., Crucifix, M., Mitsui, T., Wolff, E.W., 2017. A simple rule to determine which insolation cycles lead to interglacials. *Nature* 542, 427–432.
- Vaks, A., Bar-Matthews, M., Ayalon, A., Matthews, A., Frumkin, A., 2018. Pliocene–Pleistocene Palaeoclimate Reconstruction from Ashkelon Cave Speleothems, vol. 446. Geological Society Special Publications, Negev Desert, Israel, pp. 201–216.
- Vaks, A., Bar-Matthews, M., Matthews, A., Ayalon, A., Frumkin, A., 2010. Middle-late quaternary paleoclimate of northern margins of the Saharan–Arabian desert: reconstruction from speleothems of Negev desert, Israel. *Quat. Sci. Rev.* 29, 2647–2662.
- Vaks, A., Woodhead, J., Bar-Matthews, M., Ayalon, A., Cliff, R.A., Zilberman, T., Matthews, A., Frumkin, A., 2013. Pliocene–pleistocene climate of the northern margin of the Saharo–Arabian desert recorded in speleothems from the Negev desert, Israel. *Earth Planet. Sci. Lett.* 368, 88–100.
- Wade, L., 2019. Was our species in Europe 210,000 years ago? *Science* 365, 111.
- Waldmann, N., Torfstein, A., Stein, M., 2010. Northward intrusions of low- and mid-latitude storms across the Saharo–Arabian belt during past interglacials. *Geology* 38, 567–570.
- Weyhenmeyer, C.E., Burns, S.J., Waber, H.N., Aeschbach-Hertig, W., Kipfer, R., Loosli, H.H., Matter, A., 2000. Cool glacial temperatures and changes in moisture source recorded in Oman groundwaters. *Science* 287, 842–845.
- Weyhenmeyer, C.E., Burns, S.J., Waber, H.N., Macumber, P.G., Matter, A., 2002. Isotope study of moisture sources, recharge areas, and groundwater flow paths within the eastern Batinah coastal plain, Sultanate of Oman. *Water Resour. Res.* 38, 2–1–2–22.
- Williams, M.A.J., Duller, G.A.T., Williams, F.M., Woodward, J.C., Macklin, M.G., El Tom, O.A.M., Munro, R.N., El Hajaz, Y., Barrows, T.T., 2015. Causal links between Nile floods and eastern Mediterranean sapropel formation during the past 125 kyr confirmed by OSL and radiocarbon dating of Blue and White Nile sediments. *Quat. Sci. Rev.* 130, 89–108.
- Woodhead, J., Hellstrom, J., Maas, R., Drysdale, R., Zanchetta, G., Devine, P., Taylor, E., 2006. U-Pb geochronology of speleothems by MC-ICPMS. *Quat. Geochronol.* 1, 208–221.
- Woodhead, J., Hellstrom, J., Pickering, R., Drysdale, R., Paul, B., Bajo, P., 2012. U and Pb variability in older speleothems and strategies for their chronology. *Quat. Geochronol.* 14, 105–113.
- Zabel, M., Schneider, R.R., Wagner, T., Adegbie, A.T., De Vries, U., Kolonic, S., 2001. Late quaternary climate changes in central Africa as inferred from terrigenous input to the Niger fan. *Quat. Res.* 56, 207–217.